

2020-12

Transient sensor errors and their impact on fixed-bed regenerator (FBR) testing standards

Ramin, Hadi

Taylor and Francis

Hadi Ramin, Easwaran N. Krishnan, Gurubalan Annadurai, Wahab O. Alabi & Carey J.

Simonson (2021) Transient sensor errors and their impact on fixed-bed regenerator (FBR)

testing standards, *Science and Technology for the Built Environment*, 27:5, 656-678, DOI: 10.1080/23744731.2020.1846428

<https://hdl.handle.net/10388/14882>

<https://doi.org/10.1080/23744731.2020.1846428>

This is an Accepted Manuscript of an article published by Taylor & Francis in *Science and*

Technology in Build Environment on 14 December 2020, available at: <https://doi.org/10.1080/23744731.2020.1846428>.

Downloaded from HARVEST, University of Saskatchewan's Repository for Research

Transient sensor errors and their impact on fixed-bed regenerator (FBR) testing standards

Fixed-bed regenerators (FBRs) are a favourable option for energy recovery in building HVAC systems due to their high sensible effectiveness. Unlike other types of energy recovery exchangers, the air temperature at the outlet of FBRs varies with time, which creates challenges when measuring the outlet temperature and effectiveness of FBRs since the actual outlet air temperature will include the transient response of the FBR and the temperature sensor. In this paper, a validated numerical model of FBRs that takes into account the sensor response is used to quantify the temperature and effectiveness errors that result due to sensors response characteristics over a wide range of design parameters. The main contribution of this paper is the practical recommendations for the temperature measurement for different types of FBRs developed for HVAC applications. The recommendations presented in this paper could be implemented in future versions of the current standards (ASHRAE 84 and CSA C439-18 standards) for performance testing of air to air energy exchangers.

Keywords: Fixed-bed regenerators (FBRs), temperature measurement, sensor transient response, test standards (ASHRAE standard 84 and CSA C439-18 standard), air-to-air energy exchangers.

Nomenclature

<p>A_g cross-sectional area of the airflow duct, m^2</p> <p>A_m matrix cross-sectional area, m^2</p> <p>$A_{m,c}$ cold side matrix cross-sectional area, m^2</p> <p>$A_{m,h}$ hot side matrix cross-sectional area, m^2</p> <p>A_s heat transfer surface area of exchanger channel, m^2</p> <p>A_{ht} heat transfer surface area, m^2</p> <p>$C_{p,m}$ specific heat capacity of matrix, $J/(kg \cdot K)$</p> <p>$C_{p,g}$ specific heat capacity of air, $J/(kg \cdot K)$</p> <p>$C_{p,ts}$ specific heat capacity of sensor, $J/(kg \cdot K)$</p> <p>C^* heat capacity rate ratio</p> <p>Cr^* matrix heat capacity ratio</p> <p>$C_{r,h}^*$ hot side matrix heat capacity ratio</p> <p>$C_{r,c}^*$ cold side matrix heat capacity ratio</p> <p>$C_{p,ts}$ specific heat capacity of temperature sensor, $J/(kg \cdot K)$</p> <p>D_h hydraulic diameter, m</p> <p>h convective heat transfer coefficient, $W/(m^2 \cdot K)$</p> <p>$(hA_s)^*$ convective conductance ratio</p> <p>kg thermal conductivity of air, $W/(m \cdot K)$</p> <p>k_m thermal conductivity of matrix, $W/(m \cdot K)$</p> <p>L length of the heat exchanger, m</p> <p>Max maximum</p> <p>Min minimum</p> <p>$(\dot{m}C_p)_h$ hot airstream heat capacity rate, W/K</p> <p>$(\dot{m}C_p)_c$ cold airstream heat capacity rate, W/K</p> <p>m integer</p> <p>NTU number of transfer units</p> <p>NTU_o overall number of transfer units</p> <p>ntu_c cold side NTU</p> <p>ntu_h hot side NTU</p> <p>P total cycle time, s</p> <p>Re Reynolds number</p> <p>P_c cooling period duration, s</p> <p>P_h heating period duration, s</p> <p>Pr Prandtl number</p> <p>T_g airstream temperature, $^{\circ}C$</p> <p>$T_{c,i}$ cold inlet airstream temperature, $^{\circ}C$</p> <p>$\bar{T}_{c,o}$ time-averaged cold airstream outlet temperature, $^{\circ}C$</p> <p>$T_{c,o}$ cold airstream outlet temperature, $^{\circ}C$</p> <p>$T_{h,i}$ hot inlet airstream temperature, $^{\circ}C$</p> <p>$\bar{T}_{h,o}$ time-averaged hot airstream outlet temperature, $^{\circ}C$</p>	<p>$T_{h,o}$ hot airstream outlet temperature, $^{\circ}C$</p> <p>T_m matrix temperature, $^{\circ}C$</p> <p>T^* dimensionless temperature</p> <p>t time, s</p> <p>t_p matrix plate thickness, m</p> <p>t^* dimensionless time</p> <p>V mean airflow velocity, m/s</p> <p>V_{ts} volume of the temperature sensor, m^3</p> <p>W width of the exchanger, m</p> <p>x axial coordinate, m</p> <p>X^* dimensionless distance</p> <p>Greek symbols</p> <p>β symbolic function</p> <p>ΔT_{actual} actual temperature swing, $^{\circ}C$</p> <p>ΔT_{sensor} sensor measurement temperature swing, $^{\circ}C$</p> <p>$\Delta \varepsilon$ effectiveness error (%)</p> <p>ε effectiveness (%)</p> <p>λ conduction parameter</p> <p>λ_c cold side conduction parameter</p> <p>λ_h hot side conduction parameter</p> <p>ρ_g air density, kg/m^3</p> <p>ρ_m matrix density, kg/m^3</p> <p>ρ_{ts} temperature sensor density, kg/m^3</p> <p>τ_s sensor time constant, s</p> <p>τ_s^* dimensionless time constant</p> <p>φ symbolic function</p> <p>ACRONYMS</p> <p>AAEE air to air energy exchanger</p> <p>BC boundary condition</p> <p>EX exchanger</p> <p>EA exhaust air</p> <p>FBR fixed-bed regenerator</p> <p>HVAC heating, ventilating and air conditioning</p> <p>SA supply air</p> <p>S summer</p> <p>W winter</p>
---	--

1 Introduction

The building sector is responsible for about 40% of the total global energy consumption and more than 30% of global CO₂ emissions [1]. Heating, ventilating, and air conditioning (HVAC) systems consume a substantial part of the energy used in buildings. For instance, space cooling (70%) dominates the building energy consumption in the Middle East region [2,3], and space heating is the major contributor (60%) of Canada's building energy consumption [4].

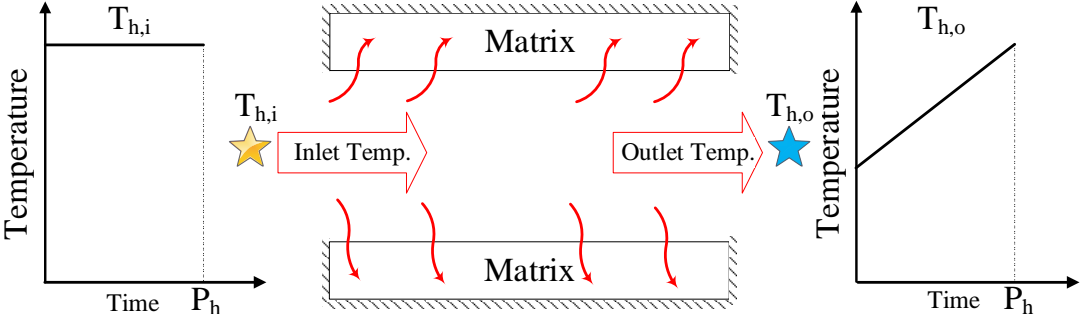
The energy required for ventilation air is critical due to increasing air-tightness and improving building envelopes [5]. Considering the energy consumption of HVAC systems and the importance of ventilation on the health and productivity of buildings' occupants [6], recovering energy from the exhaust air becomes essential for energy efficiency in buildings. Thus, various types of air-to-air energy recovery exchangers have been incorporated into the HVAC systems to help with this recovery [7].

Fixed-bed regenerators (FBRs) have recently been the subject of several studies for energy recovery in HVAC applications [8,9,18–24,10–17] because of their advantages of high ratio of heat transfer area to volume and high heat transfer effectiveness. In literature, FBRs are referred to as single-core regenerators, double-core regenerators [25], room-based ventilators [10,11], reversing-flow regenerators [25], and exchanger with a periodic change in the flow direction [13,14,19].

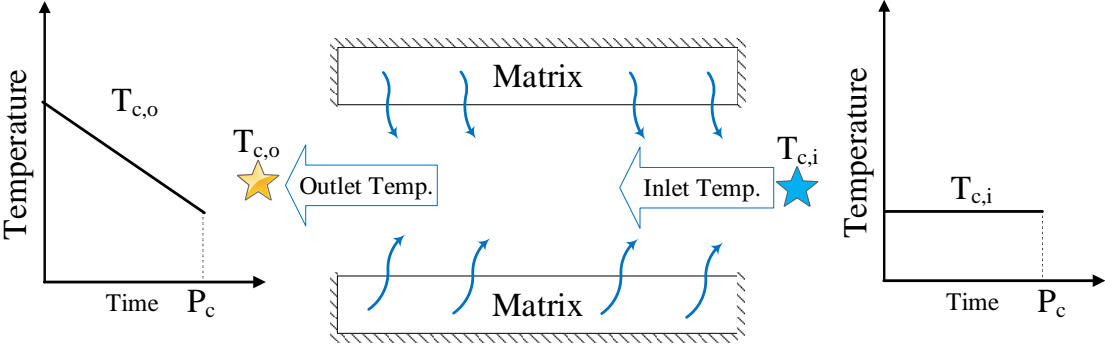
FBR is an energy exchanger with one or two stationary matrixes that store/reject heat as hot/cold air flows through the matrixes alternately, as shown in Fig. 1. This alternate heating and cooling processes in FBRs cause the outlet air temperature of FBRs to vary linearly with time [20,23]. Figure 1 presents the FBR's inlet and outlet air temperatures during the heating (P_h) and cooling (P_c) periods. After many cycles, the outlet temperature of

an FBR reaches a quasi-steady-state condition where the outlet temperature profile will be the same for every cycle [21]. The variation of the outlet air temperature (even at the quasi-steady-state condition) poses challenges for measuring the air temperature and, consequently, the effectiveness. This is due to the transient characteristics of the sensor, which causes the measured temperature to lag the actual temperature [22,23,26].

(a) Heating period



(b) Cooling period



★ ★ Temperature sensors

Figure 1. Schematic of inlet and outlet temperatures during alternate heating and cooling periods of FBRs

In addition to the temperature variation during a period, the exposure of the temperature sensors to different temperature conditions in the previous period affects their temperature measurement in the subsequent period. For example, Fig. 1 shows that the sensor measures the outlet temperature during the cold period ($T_{c,o}$) was previously exposed to the

hot inlet air ($T_{h,i}$) during the previous hot period. Therefore, both the initial condition of the sensor and the slope of the temperature profiles are critical in obtaining the effect of sensor transient characteristics in the temperature measurement [20,27–29]. With a small-scale test facility, Krishnan et al. [23] and Ramin et al. [22] studied the effects of the location of temperature sensors on the performance evaluation of FBRs for HVAC applications. For a thermocouple with a time constant of 1.5 seconds and a short recovery period (7.5 seconds), their results showed that a maximum of 15% error in effectiveness estimation occurs, which is due to the transient response of temperature sensors. However, further studies are required to provide more values to inform experiments and test standards. Ramin et al. [20] presented an analytical solution for the response of a sensor exposed to a semi-sawtooth profile. Although this solution is complicated and requires the knowledge of slope and intercept of the outlet air temperature of FBR (from numerical solution); also this solution needs to be expanded to cover all types of FBRs.

ASHRAE standard 84 [26] and CSA C439-18 standard [25] have been recently updated to include FBR performance testing. Both standards require a sampling rate that leads to collecting at least 30 temperature samples per recovery period (the recovery period is assumed to be 60 seconds). The temperature must be measured using instruments that have a response time shorter than the sampling rate. However, the temperature measurement sensors' requirements mentioned in these standards have not been studied and validated. It is also recommended in the ASHRAE standard 84 and CSA C439-18 standard to continue the testing of FBRs for one hour before reaching the quasi-steady state condition. This recommendation has been previously studied and verified for a wide range of operation

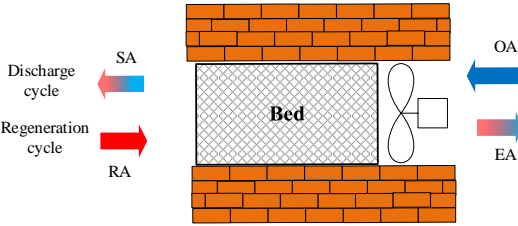
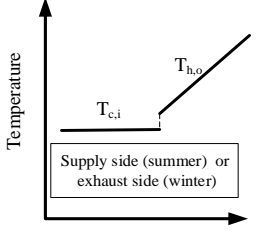
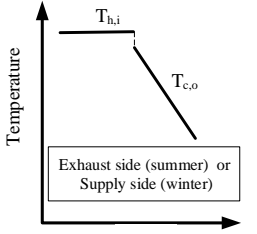
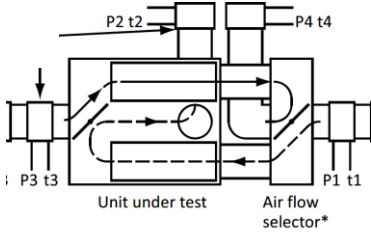
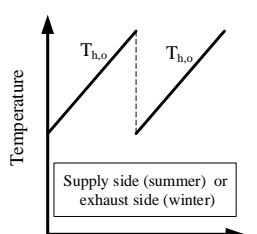
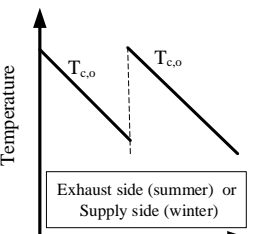
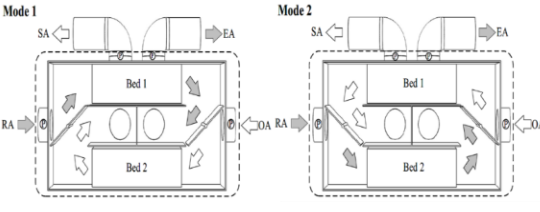
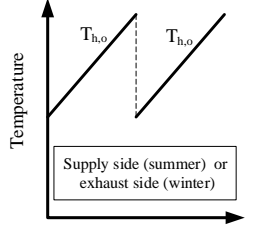
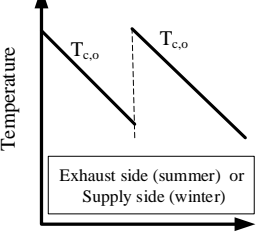
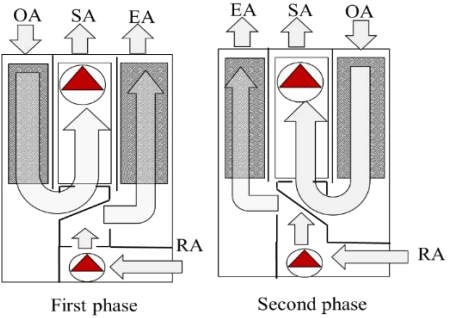
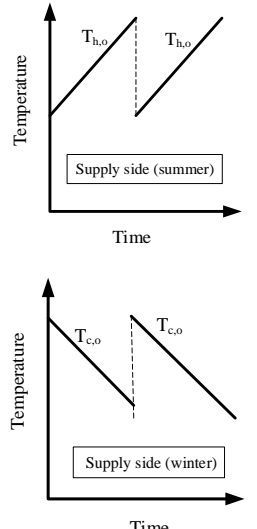
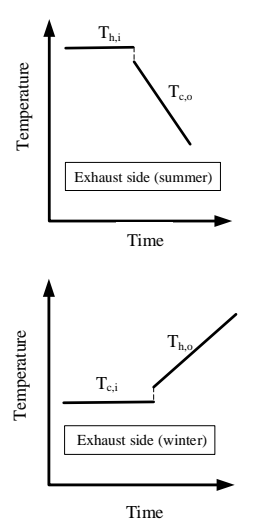
conditions [24]. Thus, the focus of this paper is on the impacts of temperature sensor transients characteristics on the quasi-steady-state temperature profile and effectiveness.

Hence, the main objective of this paper is to quantify the effect of sensor's transient characteristics on temperature measurements over a wide range of sensors time constants and FBR's design parameters (overall number of transfer units (NTU_o), matrix heat capacity rate ratio (Cr^*), and longitudinal conduction parameter (λ)) suitable for practical applications in HVAC systems. This paper will also examine the temperature sensor requirements in ASHRAE standard 84 [26] and CSA C439-18 standard [25].

2 FBR configurations and their outlet temperature profiles

FBRs can be broadly classified as single and double-core exchangers, and its outlet temperature profiles depend on the configuration, as summarized in Table 1. This table summarizes the different designs of FBRs reported in the literature [10,30], along with test standards [25,26]. The summer and winter temperature profiles at the outlet of exchangers are also presented on the supply and exhaust sides in Table 1. The temperature profiles are provided for two consecutive periods of exposure of the sensor to illustrate the initial temperature condition before each heating/cooling period. For the single-core exchanger or room-based heat recovery exchanger (ventilator) [8], as shown in the first row of Table 1, the sensors at the outlet of the supply and exhaust side of the exchanger are exposed to a periodic positive/negative (depending on the season) semi-sawtooth temperature profile.

Table 1. Different configurations of FBRs and their corresponding winter (W) and summer (S) outlet temperature profiles at the supply side (SA) and exhaust side (EA)

#	Ref.	FBR configuration	Outlet temperature profile on the SA and EA sides	
1	Nizovtsev et al.[10]			
2	CSA C439-18 standard [25]	 <p>t: Temp. Sensors</p>		
3	ASHRAE standard 84 [26]			
4	Tempeff North America Ltd. [30]			

For the double-core exchangers, as presented in the CSA C439-18 standard [25] and ASHRAE standard 84 [26], sensors at the outlet of supply or exhaust airstreams are exposed to periodic positive/negative sawtooth temperature profiles, depending on the season. On the other hand, the double-core exchanger developed by Tempeff North America [30] experiences a periodic sawtooth and semi-sawtooth temperature profiles on the supply and exhaust side of the exchanger, respectively. Compare to the sawtooth profile; the semi-sawtooth profile has a flatten part before a positive/negative ramp.

Based on the shape of the temperature profile at the outlet of the exchanger, FBRs can be classified into three main types as follows;

1. Single-core FBRs with a semi- sawtooth function (configuration 1 in Table 1): The temperature sensors are exposed to positive/negative (depending on the season) semi-sawtooth temperature.
2. Double-core FBRs with a sawtooth profile (configurations 2 and 3 in Table 1): The temperature Sensors are periodically exposed to a positive/negative (depending on the season) sawtooth temperature profile.
3. Double-core with combined sawtooth and semi-sawtooth temperature profiles (configuration 4 in Table 1): This is a combination of type 1 and 2 FBRs with respect to the temperature profile.

Thus, it can be concluded that the temperature sensors are exposed to either a positive/negative sawtooth or semi-sawtooth profile depending on the configuration of FBRs and season.

3 Numerical model and experimental test facility

Although there are correlations in the literature to calculate the effectiveness of thermal regenerators [31–33], there is no straightforward method to obtain the instantaneous temperature profile within the recovery and regeneration periods of FBRs at different design conditions. This instantaneous temperature profile during each period is essential to quantify the error due to the transient response of temperature sensors. In this paper, a validated numerical model by Ramin et al. [22] is used to obtain that temperature profile and determine the sensor effect on temperature measurement. The air streams will be referred to as hot and cold airstreams hereafter for ease of understanding and to avoid over mentioning the season.

3.1 Performance parameter

The performance of an FBR is quantified using effectiveness, which is defined as the ratio of the actual to the maximum possible heat transfer rate [25,26], and mathematically represented by Eqns. (1) and (2) for the hot side and cold period, respectively:

$$\varepsilon_h = \frac{\dot{m}_h C_p (\bar{T}_{h,o} - T_{h,i})}{\min(C_h, C_c) (T_{h,i} - T_{c,i})} \quad (1)$$

$$\varepsilon_c = \frac{\dot{m}_c C_p (\bar{T}_{c,o} - T_{c,i})}{\min(C_h, C_c) (T_{h,i} - T_{c,i})} \quad (2)$$

where \dot{m}_h and \dot{m}_c are the mass flow rate of the hot and cold airstreams, respectively. The temperature of the air leaving FBR varies with time, hence $\bar{T}_{c,o}$ and $\bar{T}_{h,o}$ are the time-averaged cold and hot temperatures, respectively. These temperatures are obtained using Eqns. (3) and (4):

$$\bar{T}_{c,o} = \frac{1}{P_c} \int_0^{P_c} T_{c,o} dt, \quad (3)$$

$$\bar{T}_{h,o} = \frac{1}{P_h} \int_0^{P_h} T_{h,o} dt \quad (4)$$

3.2 Governing equations

An FBR consists of many channels through which hot and cold airflows flow alternatively. A schematic diagram of a cross-section of a representative channel is shown in Fig. 2, along with the heat transfer process during the heating and cooling periods.

The one-dimensional governing energy equations for the airflow (subscript ‘g’) and matrix (subscript ‘m’), are presented as follows (Eqns. 5 and 6);

$$\rho_g C_{P_g} A_g \frac{\partial T_g}{\partial t} + V \rho_g C_{P_g} A_g \frac{\partial T_g}{\partial x} + h \frac{A_s}{L} (T_g - T_m) = \frac{\partial}{\partial x} \left(k_g A_g \frac{\partial T_g}{\partial x} \right) \quad (5)$$

$$\rho_m C_{P_m} A_m \frac{\partial T_m}{\partial t} - h \frac{A_s}{L} (T_g - T_m) - \frac{\partial}{\partial x} \left(k_m A_m \frac{\partial T_m}{\partial x} \right) = 0 \quad (6)$$

The boundary conditions are also presented in Eqns. (7)-(9).

$$T_g(x = 0, mP \leq t \leq mP + P_h) = T_{h,i}; \quad m = 0, 1, 2, \dots \quad (7)$$

$$T_g(x = L, mP + P_h \leq t \leq (m + 1)P) = T_{c,i}; \quad m = 0, 1, 2, \dots \quad (8)$$

$$\left. \frac{\partial T_m}{\partial x} \right|_{x=0} = \left. \frac{\partial T_m}{\partial x} \right|_{x=L} = 0 \quad (9)$$

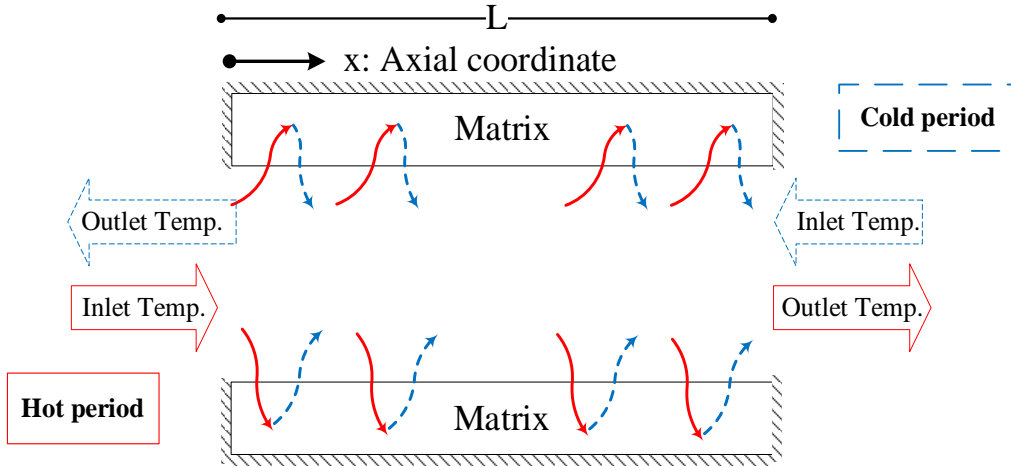


Figure 2. A schematic of the numerical domain for heat transfer in a representative channel of FBR

All symbols used in these equations are presented in the nomenclature. Also, for many practical applications, P_h and P_c are equal, and hence, they are considered to be equal in this

paper as well. The transient transport equations for the conservation of energy in the airflow and matrix (Eqns. 5 & 6) are discretized using a finite volume method [34]. A Matlab code is developed to solve the set of algebraic equations. Further details on the numerical model, grid independency test, and validations are provided in the previous publication [22].

The importance of using the dimensionless equations is that the dimensionless temperature will be independent of the selection of the hot and cold flow temperatures. Thus, errors due to the transient response of sensors will be quantified, regardless of the choice of the hot or cold temperatures, hence independent of the climate conditions. Utilizing the dimensionless variables from Table 2, the matrix and air energy equations for the hot flow and cold flow periods transform to Eqns. (10 and 11) and (12 & 13), respectively [35], subject to boundary conditions (BCs) and inlet conditions highlighted in Eqns. (14)-(16).

$$\frac{\partial T_m^*}{\partial t^*} = \frac{ntu_h}{C_{r,h}^*} (T_h^* - T_m^*) + \frac{\lambda_h}{C_{r,h}^*} \frac{\partial^2 T_m^*}{\partial X^{*2}} \quad (10)$$

$$\frac{\partial T_h^*}{\partial X^*} = ntu_h (T_w^* - T_h^*) \quad (11)$$

$$\frac{\partial T_m^*}{\partial t^*} = \frac{ntu_c}{C_{r,c}^*} (T_m^* - T_c^*) + \frac{\lambda_c}{C_{r,c}^*} \frac{\partial^2 T_m^*}{\partial X^{*2}} \quad (12)$$

$$\frac{\partial T_c^*}{\partial X^*} = ntu_c (T_c^* - T_w^*) \quad (13)$$

BCs and inlet conditions are:

$$\left. \frac{\partial T_m^*}{\partial X^*} \right|_{X^*=0} = \left. \frac{\partial T_m^*}{\partial X^*} \right|_{X^*=L} = 0 \quad (14)$$

$$T_h^*(X^* = 0, 2m \leq t^* \leq 2m + 1) = 1 \quad (15)$$

$$T_c^*(X^* = 1, 2m + 1 \leq t^* \leq 2m + 2) = 1 \quad (16)$$

From the above equations, the dimensionless temperature will be a function of several dimensionless variables, as presented in Eqn. (17):

$$T_h^* \text{ or } T_c^* = \phi(X^*, t^*, ntu_h, ntu_c, C_{r,h}^*, C_{r,c}^*, \lambda_c, \lambda_h) \quad (17)$$

The dimensionless parameters for the hot and cold airflows can be combined into overall dimensionless parameters presented in Table 2 [35]. Therefore, the dimensionless temperatures (Eqn. (17)) becomes a function of seven independent dimensionless variables, as presented in Eqn. (18):

$$T_h^* \text{ or } T_c^* = \beta(X^*, t^*, NTU_o, C^*, C_r^*, (hA)^*, \lambda) \quad (18)$$

In most HVAC practical applications, $(hA)^* = 1$; thus dimensionless temperatures for the effectiveness calculation (at the outlet of FBRs $X^* = 0$ and 1) becomes a function of four parameters (NTU_o, C^*, C_r^* and, λ).

Table 2: Dimensionless variables and parameters for heat transfer in FBRs

Dimensionless variables	Length	time	
	$X^* = \frac{x}{L}$	$t^* = \frac{t}{P_h}$	
	Hot side temperature	Cold side temperature	Matrix temperature
	$T_h^* = \frac{T_h - T_{c,i}}{T_{h,i} - T_{c,i}}$	$T_c^* = \frac{T_c - T_{c,i}}{T_{h,i} - T_{c,i}}$	$T_m^* = \frac{T_m - T_{c,i}}{T_{h,i} - T_{c,i}}$
Dimensionless parameters	Hot side	$ntu_h = (hA)_h / C_h$	$\lambda_h = \frac{k_m A_{m,h}}{LC_h}$
		$C_{r,h}^* = \frac{(mC_p)_m P_h}{C_h}$	$C_h = (\dot{m}C_p)_{g,h}$
	Cold side	$ntu_c = (hA)_c / C_c$	$\lambda_c = \frac{k_m A_{m,c}}{LC_c}$
		$C_{r,c}^* = \frac{(mC_p)_m P_c}{C_c}$	$C_c = (\dot{m}C_p)_{g,c}$
Overall Dimensionless parameters	$C_r^* = \frac{C_r}{\min(C_h, C_c)}$	$C^* = \frac{\min(C_h, C_c)}{\max(C_h, C_c)}$	$NTU_o = \frac{1}{\min(C_h, C_c)} \left[\frac{1}{(hA)_h} + \frac{1}{(hA)_c} \right]^{-1}$
	$\lambda = \frac{\lambda_c C_c + \lambda_h C_h}{\min(C_c, C_h)}$	$(hA)^* = \frac{(hA) \text{ on the } \min(C_h, C_c) \text{ side}}{(hA) \text{ on the } \max(C_h, C_c) \text{ side}}$	

From the definition of the dimensionless variables, the effectiveness of FBR in Eqns.

(3) & (4) simplifies to Eqn. (19) and (20) for $C_{min} = C_c$:

$$\epsilon_c = \bar{T}_{c,o}^* \quad (19)$$

$$\epsilon_h = \frac{1 - \bar{T}_{h,o}^*}{C^*} \quad (20)$$

In many practical applications and the test standards (CSA C439-18 standard [25] and ASHRAE standard 84 [26]), the flow in regenerators are considered to be balanced ($C^* = \frac{C_c}{C_h} = 1$), and hence the results are presented for such a balanced flow condition.

Temperature sensors usually have a small mass, which makes the lumped capacitance method applicable [36] for the corresponding transient energy balance. The energy balance for the sensors is presented in Eqn. (21);

$$\frac{dT_s}{dt} = \frac{1}{\tau_s} (T_g - T_s) \quad (21)$$

where τ_s is the time constant of the temperature sensor, and T_s is the temperature that the sensor records. Equation (21) can be rewritten using the dimensionless variables as Eqn. (22);

$$\frac{dT_s^*}{dt^*} = \frac{P_h}{\tau_s} (T_g^* - T_s^*) = \frac{1}{\tau_s^*} (T_g^* - T_s^*) \quad (22)$$

where τ_s^* is the time constant to recovery period ratio (dimensionless time constant of temperature sensor), and is mathematically depicted by Eqn. (23):

$$\tau_s^* = \frac{\tau_s}{P_h} \quad (23)$$

Therefore the temperature obtained from Eqn. (18) gives the actual outlet air temperature of the exchanger, and the one obtained from Eqn. (22) is what temperature sensors record.

Figure 3 (a-d) shows different possible outlet air temperature profiles from the numerical

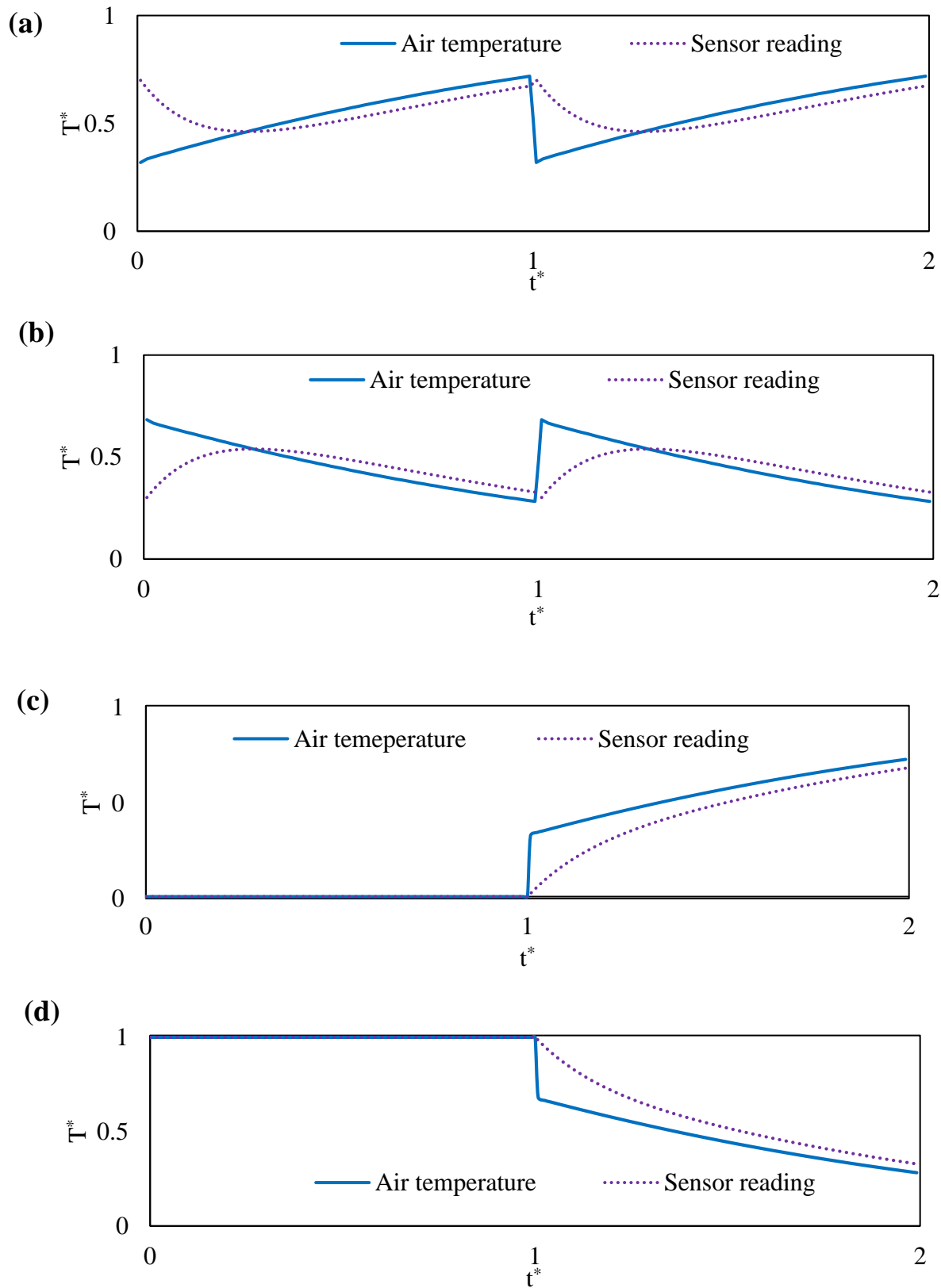


Figure 3. Outlet air temperatures of positive/negative sawtooth (a & b) and the semi-sawtooth (c & d) profile and their corresponding sensor measurements with $\tau_s^*=0.2$ ($NTU_o=1.0$, $Cr^*=1.0$, $\lambda=0$)

model (See Table 1) of FBRs along with their corresponding sensor measurements (for $\tau_s^* = 0.2$), obtained from Eqn. (22) for $NTU_o=1$, $Cr^*=1$, and $\lambda=0$.

The deviation between the average actual air temperature and the sensor recording for both positive/negative sawtooth profiles is equal. This means that effectiveness errors (a function of average outlet temperature) due to the sensor measurements are identical for the positive and negative sawtooth profiles. This conclusion is also applicable to the positive/negative semi-sawtooth profile. Therefore, in terms of error due to temperature measurement, there is no difference between positive and negative temperature profiles (either sawtooth or semi-sawtooth). Hence, in the rest of the paper, further analyses are carried out only for the positive sawtooth (heating period) (Fig. 3 (a)) and the positive semi-sawtooth temperature profiles (heating period) (Fig. 3(c)).

3.3 *FBR small-scale test facility*

A small scale test facility was used to validate the numerical model [22]. The schematic diagram of the facility is shown in Fig.4. The principle of operation, instrumentation, and data analysis procedures of the experiments are reported in previous publications of the present authors [23,37].

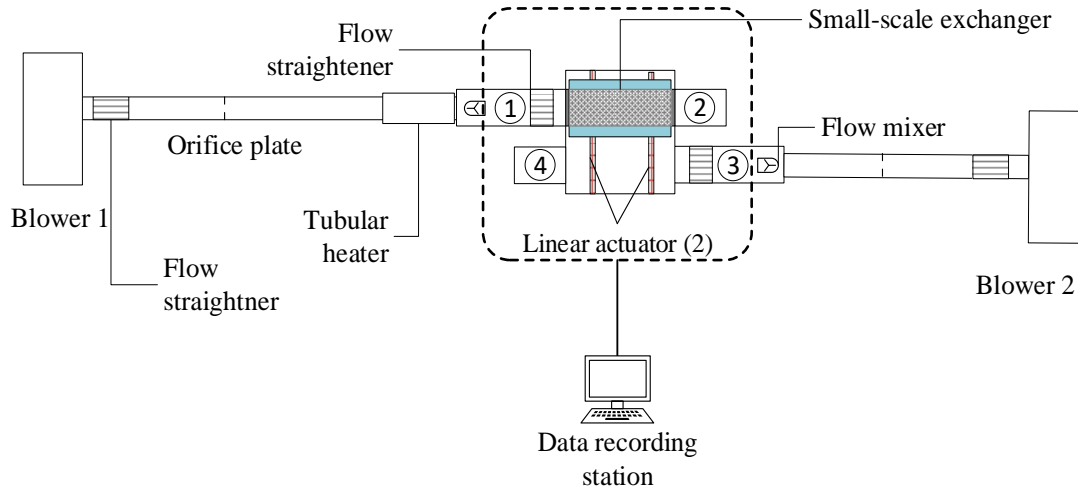


Figure 4. Schematic of the small scale test facility

The schematic of the exchanger (made of aluminum plates) and its thermo-physical properties are shown in Fig.5 and Table 3, respectively. A linear actuator unit (LAU) is used to slide the exchanger between the hot and cold airstreams to mimic the alternate heating and cooling process of FBRs. The temperature of the hot and cold airstreams is measured using calibrated T-type thermocouples (with a time constant (τ_s) of 1.5 seconds) with an uncertainty of ± 0.2 °C. The uncertainty in flow rate measurements is $\pm 2\%$. Uncertainty analysis has been performed by following the rule of error propagation [38], and the uncertainties in sensible effectiveness and normalized temperatures are 3% and 1.5%, respectively. Generalized uncertainty analysis of small-scale testing has been presented, and the contribution of errors from temperature and flow rate measurements on sensible effectiveness is reported in our previous publication [23]. Energy balance was performed, and results showed that for a wide range of test conditions, the test facility conserves energy (with a deviation of less than 5%). The experiment is continued until the exchanger attains the quasi-steady-state condition.

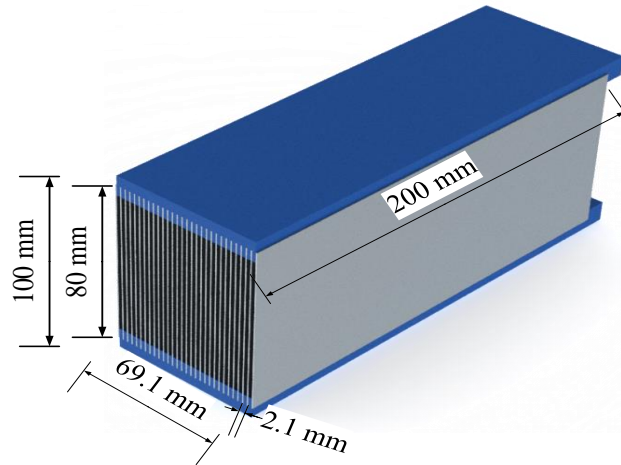


Figure 5. A schematic of the small scale exchanger

Table 3. Geometrical details, thermophysical properties of the exchanger, dimensionless parameters, and sensor time constant

Exchanger channel	Length(mm)	200
	Width (mm)	80
	Height (mm)	2.1
	Hydraulic diameter (mm)	3.5
Aluminum plates	Thickness (mm)	0.62
	Thermal conductivity (W/m·K)	2730
	Density (kg/m ³)	220
	Specific heat capacity (J/kg·K)	904
Dimensionless parameters	NTU_o	2.4
	Cr^*	1.2
	C^*	1.0
	λ	0.3
Temperature Sensor	Time constant (s)	1.5

3.4 Validation of the results

The effectiveness calculated from the literature correlations [35,39] and from the small-scale test facility is used to validate the numerical model and presented in our previous paper [22]. In the present study, the temperature profile from the numerical model (including the sensor response) is compared with the temperature profile from the small-scale test facility.

Figure 6 (a) shows the comparison of the quasi-steady-state dimensionless temperature profiles at the outlet of FBR from the small-scale experiment and the numerical model (including the sensor response) for both heating and cooling periods (60 s). From Fig.6 (a), it can be observed that the temperature from the numerical model (including the sensor response from Eqn. (22)) and the experiment are in good agreement. Therefore the numerical model is accurate in predicting the transient behavior of the outlet temperature of FBR and sensor response. The measured temperature profiles from the experiment (including sensor response) at different recovery periods are modified following the method presented in [23], and the resulted effectiveness are compared with the prediction from the numerical model; This effectiveness comparison is presented in Fig. 6(b). This figure demonstrates that the numerical model results agree with the experimental effectiveness within the uncertainty bounds. Hence, the developed numerical model can be confidently used to evaluate the performance of FBR for different operating conditions.

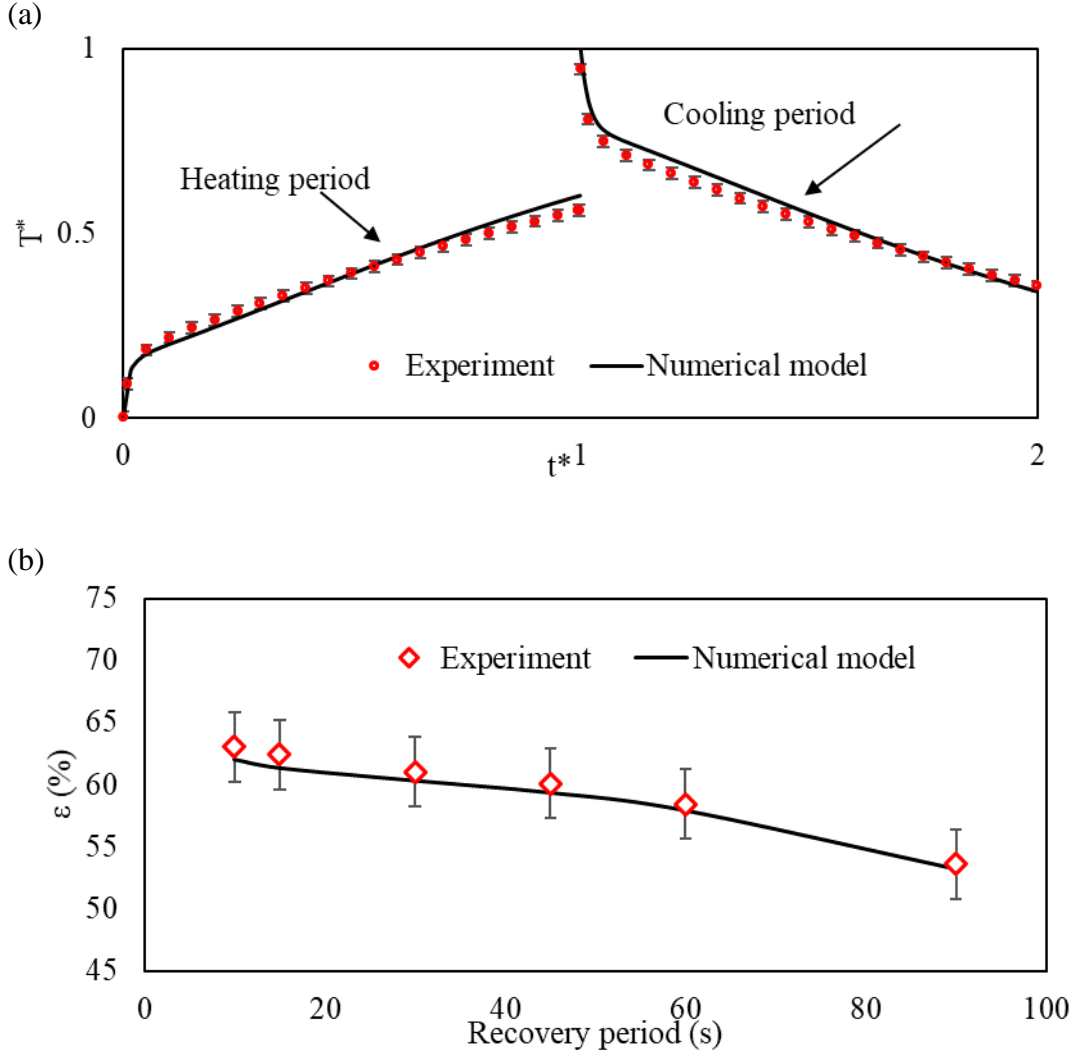


Figure 6. (a) Numerical and experimental temperature comparison from the beginning of the experiment ($NTU_o=2.4$, $Cr^*=1.2$, $\lambda=0.3$) and (b) comparison of sensible effectiveness from experiment and numerical model

4 Results and discussions

The effects of sensor time constant on the temperature measurements at the quasi-steady-state condition are discussed in detail in this section. The actual air temperature is obtained from Eqn. (18) over a wide range of NTU_o , Cr^* , and λ . The sensor temperature measurements are obtained from Eqn. (22) for different dimensionless time constant (τ_s^*). The difference between effectiveness obtained from Eqns. (18) and (22), is reported as the effectiveness error ($\Delta\epsilon$) due to the transient response of sensors (Eqn. (24)):

$$\Delta\epsilon = |\epsilon_{\text{actual}} - \epsilon_{\text{sensor}}| \quad (24)$$

4.1 FBRs with a sawtooth profile

Figure 7 (a) presents the sawtooth temperature profile at the outlet of FBRs during the quasi-steady-state condition. The temperature measurement from sensors (Eqn. (22)) with two different dimensionless time constants ($\tau_s^* = 0.2$ and 0.5) is also presented in Fig. 7 (a). For the sawtooth profile (despite different temperature profiles from sensors with different time constants), the predicted effectiveness from both sensors is calculated to be the same, and also the effectiveness from sensors is equal to the actual effectiveness. Thus, the effectiveness of FBRs with the sawtooth outlet temperature is not sensitive to the time constant of the sensor. In other words, $\Delta\epsilon$ is equal to zero at different dimensionless time constants (τ_s^*). However, the shape of the temperature profile is not precisely captured with sensors, and the temperature swing cannot be obtained accurately (ΔT_{sensor} and ΔT_{actual} in Fig. 7 (a) are presented for $\tau_s^* = 0.2$ only). Additionally, the ratio of $\Delta T_{\text{sensor}}/\Delta T_{\text{actual}}$ decreases when the time constant increases, as depicted in Fig.7 (b). In this figure, the sensor measured temperature difference over the period (temperature swing) is about 6% of the actual FBR temperature difference for $\tau_s^* = 2$. In other words, with increasing sensor time constant (to two times as recovery period), the variation of measured temperature within the period decreases significantly; however, the average measured temperature is equal to the actual average air temperature (equal effectiveness).

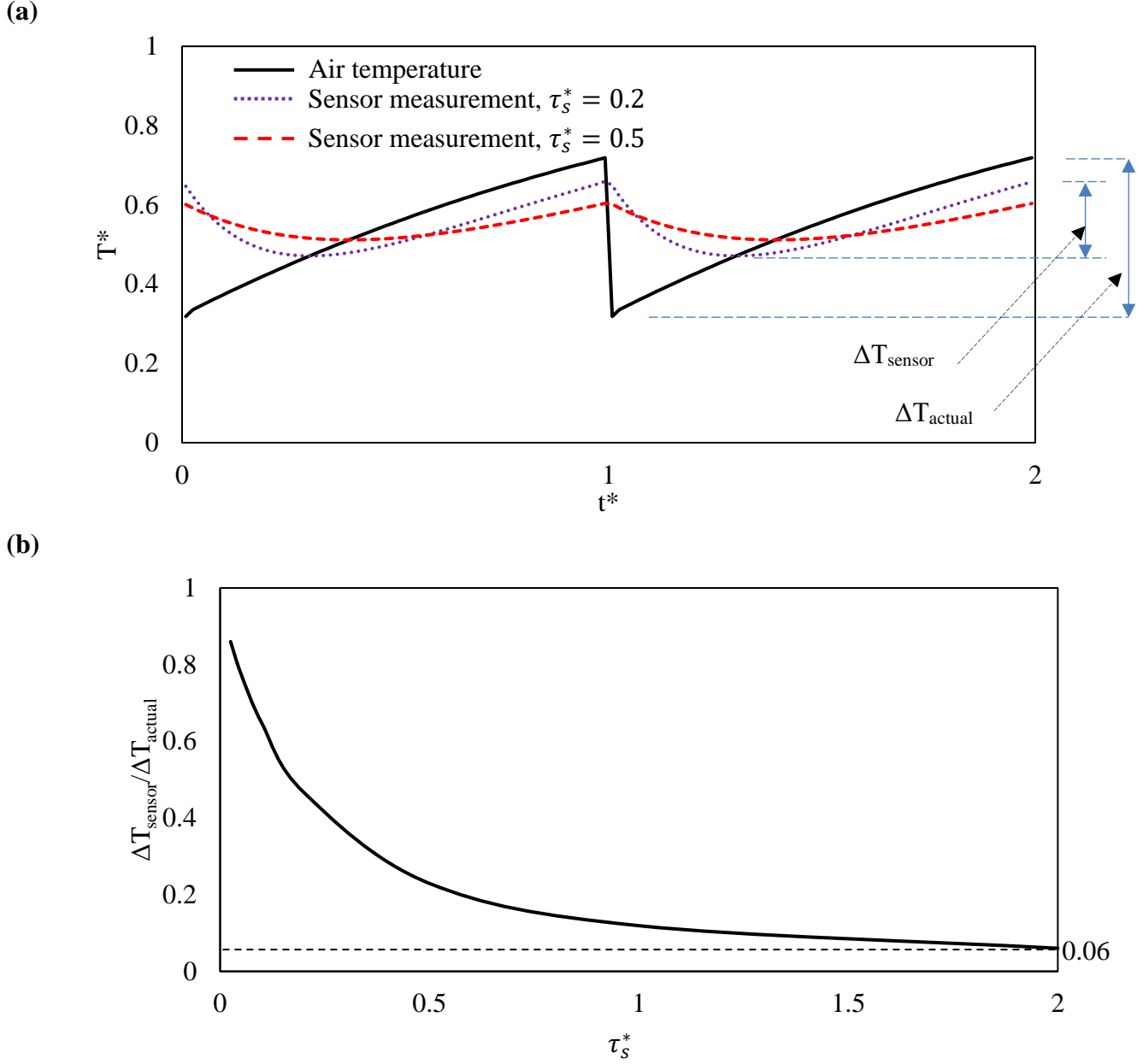


Figure 7. (a) Quasi-steady-state temperature profile and sensor measurements with two dimensionless time constant of $\tau_s^* = 0.2$ and 0.5 , and (b) $\Delta T_{sensor}/\Delta T_{actual}$ for FBR with sawtooth temperature ($NTU_o=1$, $Cr^*=1$, and $\lambda=0$)

Experiments can be designed to select the appropriate temperature sensors that capture the temperature shape (temperature swing) within a required precision. For example, Fig. 8 (a-d) shows the required τ_s^* (maximum values) to capture 90 % or 80 % of the temperature swing for FBRs with a sawtooth temperature profile over a wide range of design parameters. For example, to capture 90% of temperature swing for an FBR ($NTU_o = 5$, Cr^* and $\lambda = 0.0$),

the maximum dimensionless time constant of about 0.06 must be selected (Figure 8 (b)).

Increasing conduction parameter (λ) has a small effect on the required dimensionless time constant (τ_s^*).

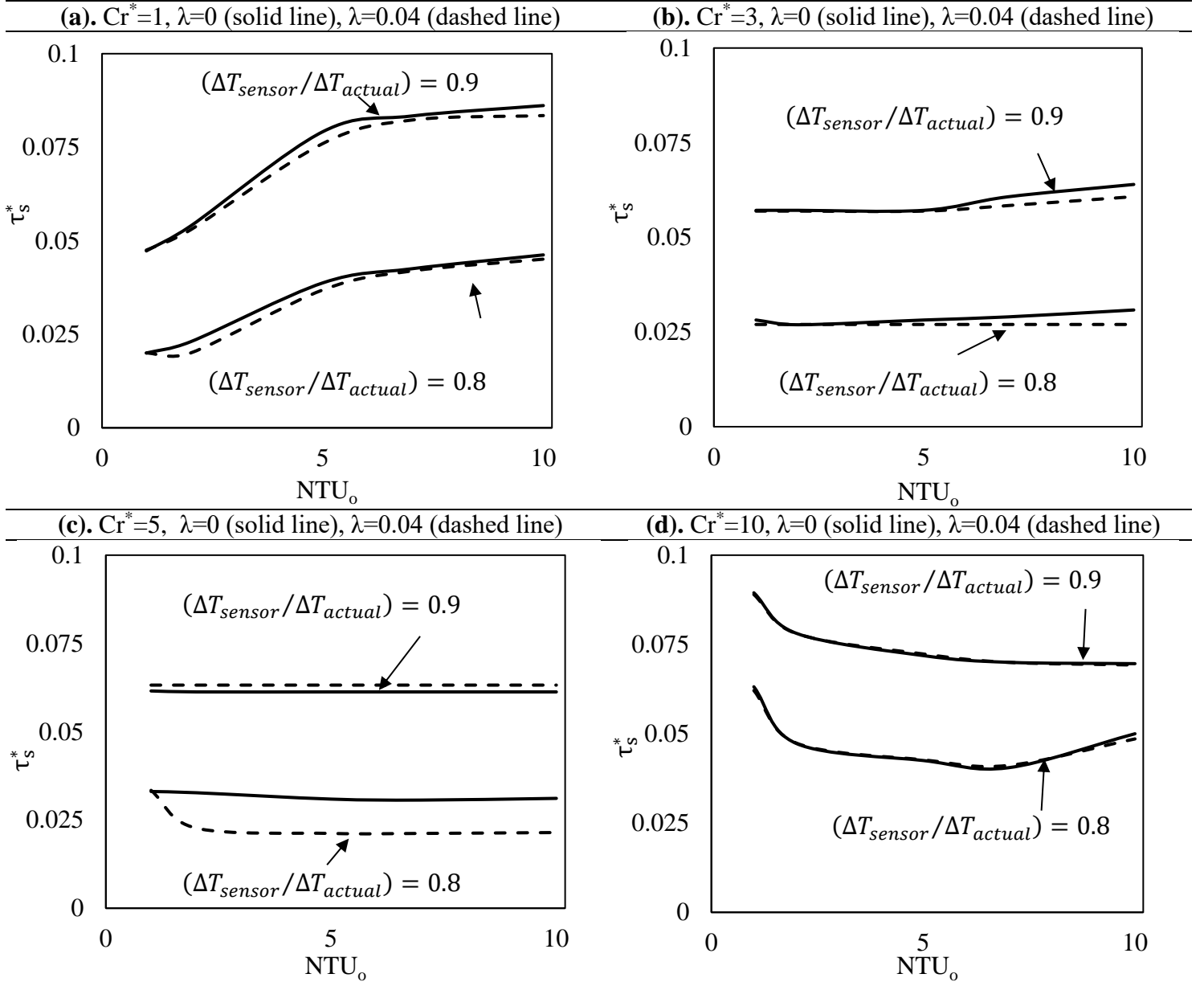


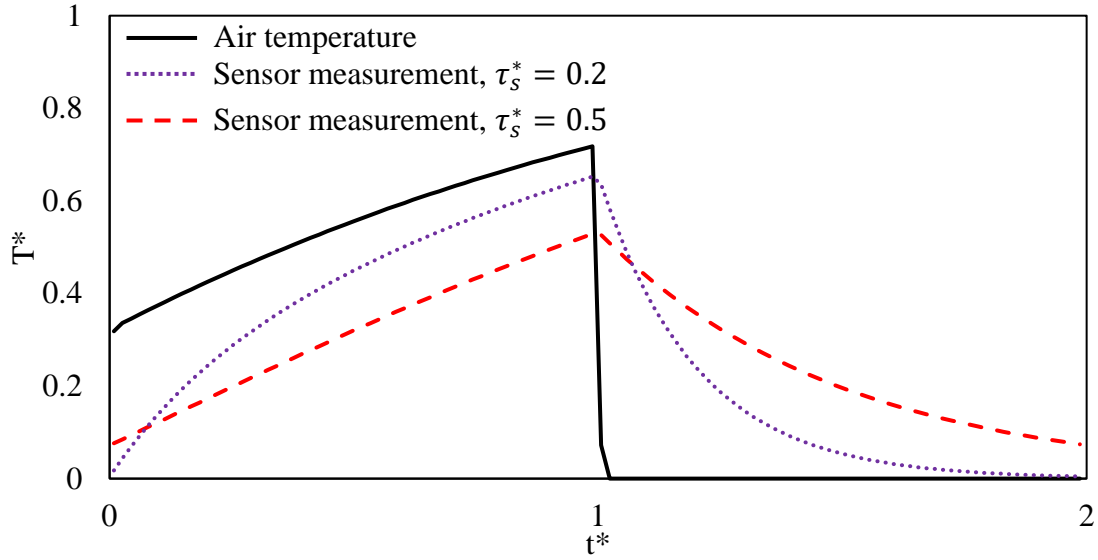
Figure 8. The required dimensionless sensor time constant (τ_s^*) to capture 80% and 90% of the actual temperature swing ($\Delta T_{sensor} / \Delta T_{actual} = 80\%$ and $\Delta T_{sensor} / \Delta T_{actual} = 90\%$) for $\lambda = 0$ (solid), 0.04 (dashed), $NTU_o = 1-10$ and $Cr^* = 1, 3, 5, 10$

4.2 FBRs with a semi-sawtooth profile

Figure 9 (a) presents the semi-sawtooth temperature profile at the outlet of FBRs during a quasi-steady-state condition. The temperature measurements from sensors with two different dimensionless time constants of $\tau_s^* = 0.2$ and 0.5 are also presented along in Fig. 9 (a). Both sensors' measurements follow the actual air temperature profile. However, the shape of the temperature profile and also the effectiveness cannot be measured accurately. Unlike FBRs with a sawtooth profile, the sensor temperature measurement does not cross the actual air temperature profile of FBRs with semi-sawtooth profiles. Therefore the calculation of the temperature swings (ΔT_{sensor} and ΔT_{actual}) does not provide any significant insight into the relationship between the sensor and the actual temperature swing. Therefore temperature swing is not discussed for FBRs with a semi-sawtooth temperature profile. Figure 9 (b) shows that the effectiveness measurements from sensors depend on the sensor time constant, and the effectiveness error increases significantly with an increase in the sensor time constant.

At the quasi-steady-state condition, the sensors exposed to a semi-sawtooth temperature profile would not measure the temperature and effectiveness correctly. Comprehensive results of effectiveness errors ($\Delta\epsilon$ in Eqn. 24) for FBRs with semi-sawtooth profile at different dimensionless time constant (τ_s^*), and longitudinal heat conduction parameter (λ) values (over a wide range of the design parameters of NTU_o and Cr^*) are presented in Appendix A. Tables A.1 to A.9 summarize the effectiveness error due to the temperature sensor response at different ranges of dimensionless design parameters and time constants. Using the values reported in those tables, one can estimate the magnitude of errors for sensors with different time constants at specific dimensionless parameters. A practical example of the application of the tables provided in Appendix A is presented in the appendix.

(a)



(b)

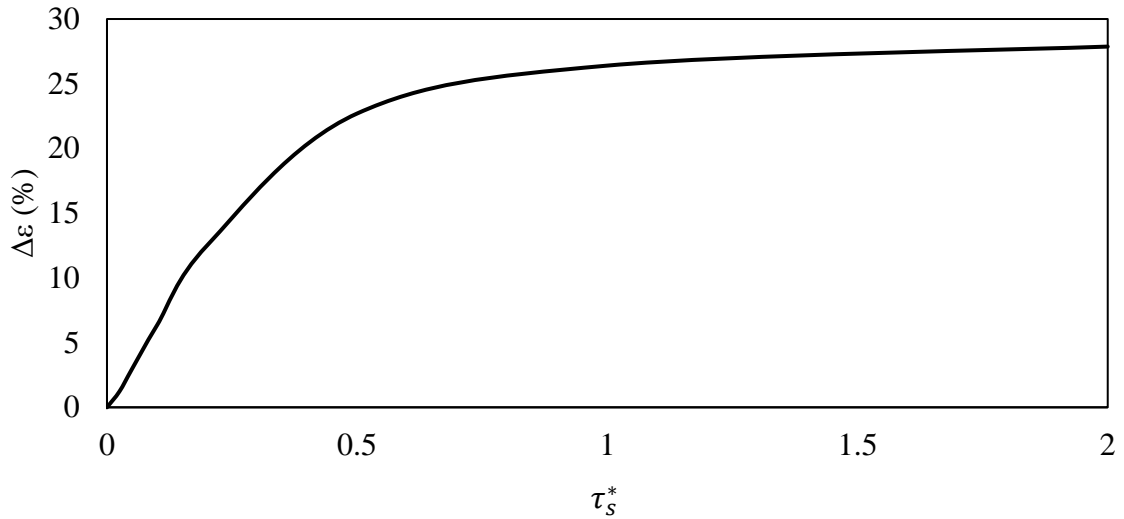


Figure 9. (a) Quasi-steady-state temperature profile and sensor measurements with two dimensionless time constant of $\tau_s^* = 0.2$ and 0.5 , and (b) effectiveness error ($\Delta \epsilon$) for FBR with semi-sawtooth temperature ($NTU_o=1$, $Cr^*=1$, and $\lambda=0$)

Figure 10 presents the effectiveness error as a function of dimensionless time constant (τ_s^*) for different design conditions ($NTU_o=1-10$ and $Cr^*=1-10$). According to Fig. 10, the effectiveness error increases with an increase in τ_s^* . At smaller NTU_o (<2) and Cr^* (<2), the effectiveness errors are significant, which becomes smaller at higher NTU_o ($=10$) and Cr^* ($=10$). The effectiveness error also increases with an increase in the longitudinal

conduction parameter (λ), and at higher $NTU_o(>5)$ and $Cr^*>5$ values, the effect of axial conduction in the matrix becomes more significant in the effectiveness error.

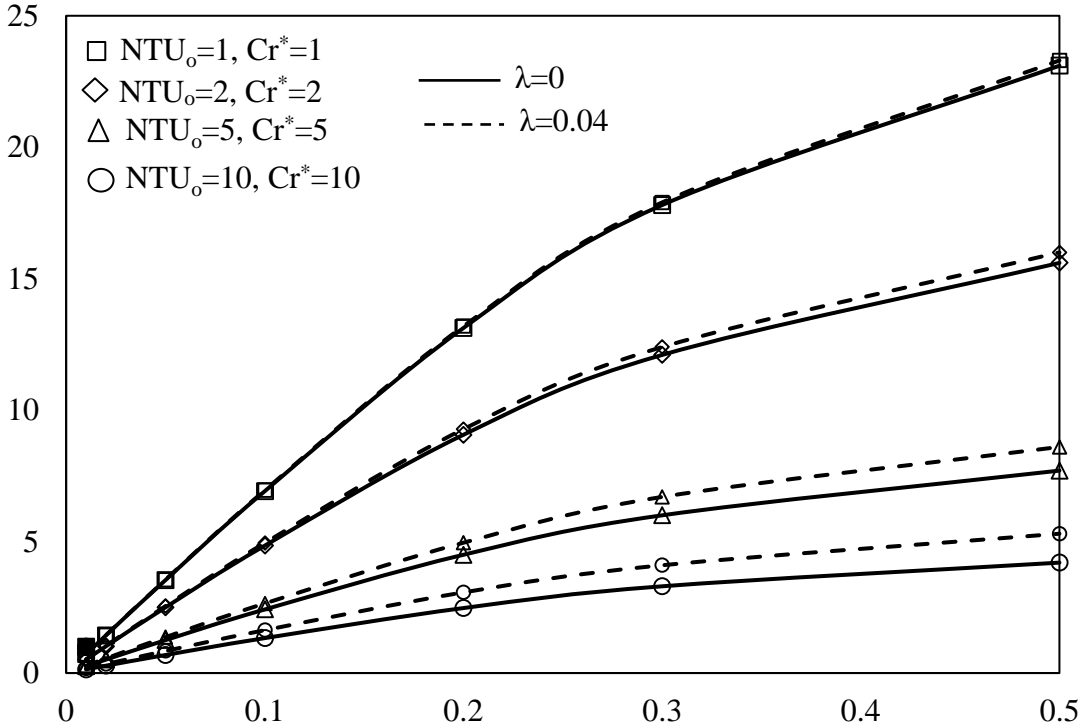


Figure 10. Effectiveness error as a function of τ_s^* at different design parameters of NTU_o and Cr^* ($\lambda=0, 0.04$)

Using the results presented in Appendix A, experiments can be designed to select sensors to maintain the effectiveness error within specific ranges. For example, Fig. 11 shows the dimensionless time constants that result in effectiveness error ($\Delta\varepsilon$) less than 1%, 2%, and 3% at different NTU_o and Cr^* values for $\lambda=0$ and 0.04. At small values of Cr^* , the dimensionless time constant (τ_s^*) needs to be smaller for a certain value of effectiveness error. And at higher values of NTU_o (keeping the same Cr^*), a sensor with higher values of dimensionless time constant could be used to have a certain effectiveness error. The results in Fig. 11 also show that more accurate (smaller sensor time constant) should be used when the conduction parameter increases.

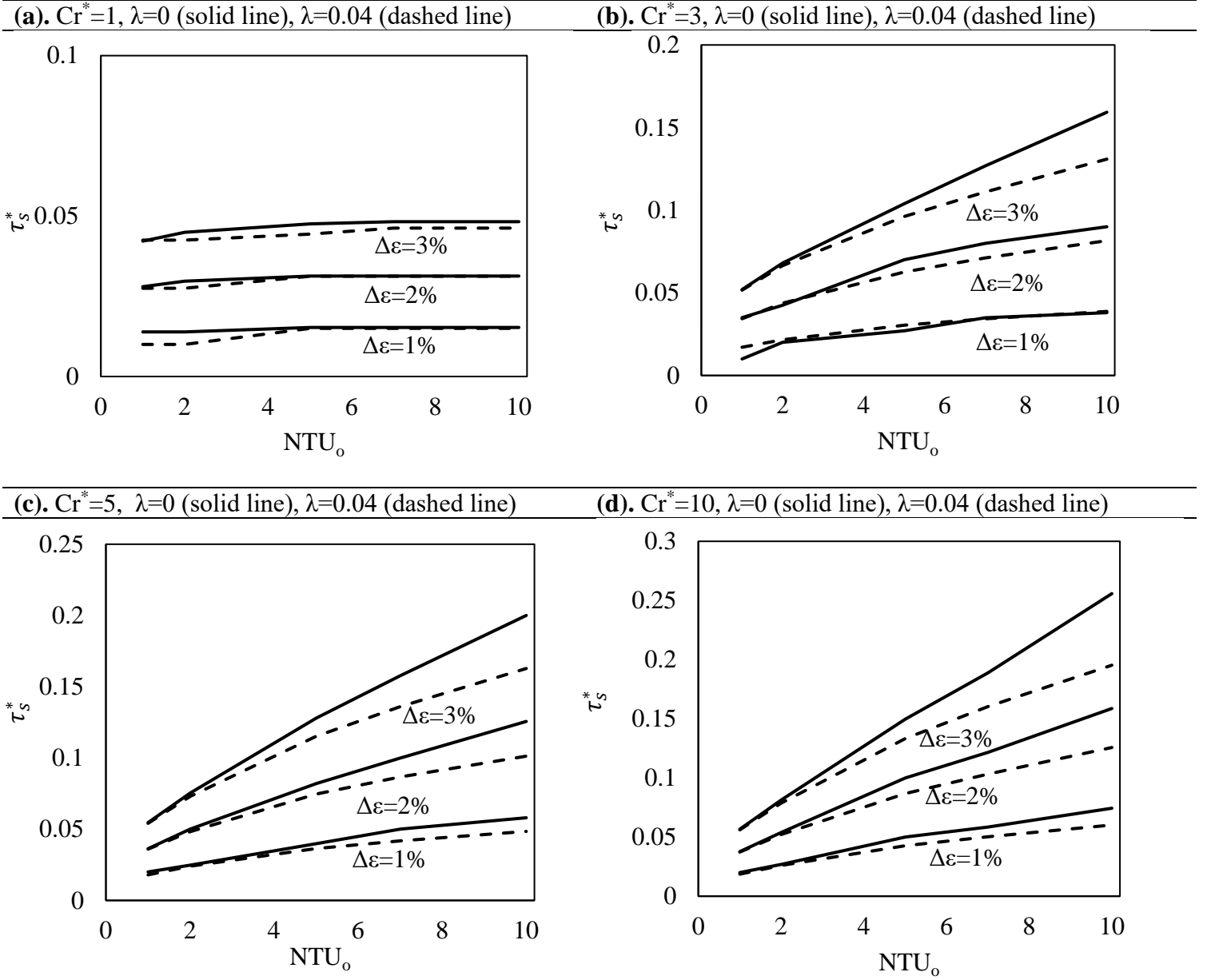


Figure 11. The required dimensionless sensor time constant (τ_s^*) that results in effectiveness error less than 1%, 2% and 3% for $NTU_o=1-10$ and $Cr^*=1, 3, 5,$ and 10

4.3 Testing Standards

ASHRAE standard 84 [26] and CSA C439-18 standard [25] do not differentiate between the FBRs with saw-tooth and semi saw-tooth outlet temperature profiles. The results obtained in this study show that the temperature sensor requirements in standards are stringent and could be relaxed for FBRs with a saw-tooth outlet temperature profile in terms

of effectiveness. Also, the results in Appendix A could be used to determine the requirements for temperature sensors of FBRs with a semi saw-tooth temperature profile. The requirements for reaching the quasi-steady-state condition in standards are also verified in the previous study of the same authors [24].

5 Conclusions

The outlet temperature of FBR varies with time both in the initial transient and subsequent quasi-steady-state conditions. Hence, it is difficult for the sensors to accurately measure the temperature variation due to (i) steep slope of temperature variation and (ii) its exposure to a different temperature condition during the previous period. This inaccurate temperature measurement affects the effectiveness evaluation during the quasi-steady-state condition. In this paper, two distinct outlet temperature profiles for FBRs of positive/negative sawtooth and semi-sawtooth profiles are identified (depending on the FBR configurations), and both profiles are analyzed for the impacts of temperature measurements using a validated numerical model.

Regardless of FBRs configurations, the ASHRAE standard 84 and CSA C439-18 standard recommend rigorous requirements for the temperature sensors to accurately determine the effectiveness of FBRs. The analysis in this paper revealed that the single-core and double-core FBRs require different considerations for temperature measurement and effectiveness determination.

The main conclusions of the present paper are as follows:

- For FBRs with a sawtooth outlet temperature profile (double-core FBRs as in the ASHRAE standard 84 and CSA C439-18 standard), the effectiveness could be accurately measured regardless of sensor time constant. However, the shape of the

temperature profile (temperature swing) cannot be captured correctly. The results in this paper provide the minimum sensor time constant to capture 80% and 90% of temperature swing over a wide range in design parameters.

- For FBRs with a semi-sawtooth temperature profile (single-core FBRs and some double-core FBRs), the effect of sensor response is significant for effectiveness estimation. The effectiveness errors due to the response of sensors at a wide range of NTU_o , Cr^* , and λ and at different dimensionless time constants (τ_s^*) are evaluated and presented in graphs (in the manuscript) and tables (Appendix A) in this paper.
- At smaller NTU_o and Cr^* , the effectiveness error due to sensor transient response increases for FBRs with a semi-sawtooth temperature profile, and this error is around 25% for small NTU_o and $Cr^* (\approx 1)$ at $\tau_s^* = 0.5$. An increase in the axial conduction in the matrix increases the effectiveness error, and the effect is more significant at higher NTU_o and Cr^* .

The test configurations in the ASHRAE standard 84 and CSA C439-18 standard produce a sawtooth temperature profile (double-core FBRs), which allows for accurate effectiveness measurement. Many double-core FBRs installations produce a sawtooth temperature profile on the supply air side, but a semi-sawtooth profile on the exhaust side. Thus, sensor time constant and selection needs careful consideration when taking field measurements on the exhaust airside.

The results of the current study will be helpful in developing standard recommendations in the future ASHRAE standard 84 and CSA C439-18 standards for testing the air to air energy exchangers.

ACKNOWLEDGMENTS

References

- [1] M.R.H. Abdel-Salam, M. Fauchoux, G. Ge, R.W. Besant, C.J. Simonson, Expected energy and economic benefits, and environmental impacts for liquid-to-air membrane energy exchangers (LAMEEs) in HVAC systems: A review, *Appl. Energy*. 127 (2014) 202–218. <https://doi.org/10.1016/j.apenergy.2014.04.004>.
- [2] H. El-Dessouky, H. Ettouney, A. Al-Zeefari, Performance analysis of two-stage evaporative coolers, *Chem. Eng. J.* 102 (2004) 255–266. <https://doi.org/10.1016/j.cej.2004.01.036>.
- [3] H. Ramin, P. Hanafizadeh, T. Ehterami, M.A. AkhavanBehabadi, Life cycle-based multi-objective optimization of wall structures in the climate of Tehran, *Adv. Build. Energy Res.* 13 (2019) 18–31. <https://doi.org/10.1080/17512549.2017.1344137>.
- [4] B. Rezaie, E. Esmailzadeh, I. Dincer, Renewable energy options for buildings: Case studies, *Energy Build.* 43 (2011) 56–65. <https://doi.org/10.1016/j.enbuild.2010.08.013>.
- [5] C.A. Roulet, F.D. Heidt, F. Foradini, M.C. Pibiri, Real heat recovery with air handling units, *Energy Build.* 33 (2001) 495–502. [https://doi.org/10.1016/S0378-7788\(00\)00104-3](https://doi.org/10.1016/S0378-7788(00)00104-3).
- [6] F. Mofidi, H. Akbari, Personalized energy costs and productivity optimization in offices, *Energy Build.* 143 (2017) 173–190. <https://doi.org/10.1016/j.enbuild.2017.03.018>.
- [7] M. Justo Alonso, P. Liu, H.M. Mathisen, G. Ge, C. Simonson, Review of heat/energy recovery exchangers for use in ZEBs in cold climate countries, *Build. Environ.* 84 (2015) 228–237. <https://doi.org/10.1016/J.BUILDENV.2014.11.014>.
- [8] V.Y. Borodulin, M.I. Nizovtsev, A criterial analysis of the effectiveness of air-to-air

- heat exchangers with a periodic change of airflow direction, *Appl. Therm. Eng.* 130 (2018) 1246–1255. <https://doi.org/10.1016/j.applthermaleng.2017.11.126>.
- [9] M.I. Nizovtsev, V.Y. Borodulin, V.N. Letushko, Influence of condensation on the efficiency of regenerative heat exchanger for ventilation, *Appl. Therm. Eng.* 111 (2017) 997–1007. <https://doi.org/10.1016/j.applthermaleng.2016.10.016>.
- [10] M.I. Nizovtsev, V.Y. Borodulin, V.N. Letushko, A.A. Zakharov, Analysis of the efficiency of air-to-air heat exchanger with a periodic change in the flow direction, *Appl. Therm. Eng.* 93 (2016) 113–121. <https://doi.org/10.1016/j.applthermaleng.2015.09.029>.
- [11] Y.A. Aristov, I. V Mezentsev, V.A. Mukhin, A new approach to heat and moisture regeneration in the ventilation system of rooms. I. Laboratory prototype of the regenerator, *J. Eng. Phys. Thermophys.* 79 (2006) 569–576. <https://doi.org/10.1007/s10891-006-0137-7>.
- [12] L. Pérez-Lombard, J. Ortiz, C. Pout, A review on buildings energy consumption information, *Energy Build.* 40 (2008) 394–398. <https://doi.org/10.1016/j.enbuild.2007.03.007>.
- [13] C.C. Chang, J. De Liang, S.L. Chen, Performance investigation of regenerative total heat exchanger with periodic flow, *Appl. Therm. Eng.* 130 (2018) 1319–1327. <https://doi.org/10.1016/j.applthermaleng.2017.11.024>.
- [14] C.C. Chang, S.L. Chen, T.Y. Lin, Y.C. Chiang, Experimental and theoretical investigation of regenerative total heat exchanger with periodic flow for air-conditioning systems, *Int. J. Refrig.* 81 (2017) 123–133. <https://doi.org/10.1016/j.ijrefrig.2017.05.015>.

- [15] C.C. Chang, W.J. Luo, C.W. Lu, Y.S. Cheng, B.Y. Tsai, Z.H. Lin, Effects of process air conditions and switching cycle period on dehumidification performance of desiccant-coated heat exchangers, *Sci. Technol. Built Environ.* 23 (2017) 81–90. <https://doi.org/10.1080/23744731.2016.1210971>.
- [16] H. Han, Y. Il Kwon, Inhaling/exhaling heat recovery ventilator using the concept of alternating-current ventilation, *HVAC R Res.* 12 (2006) 843–859. <https://doi.org/10.1080/10789669.2006.10391212>.
- [17] E. Cerrah, C. McCague, M. Bahrami, Sorbent based enthalpy recovery ventilator, *Energy Build.* 211 (2020). <https://doi.org/10.1016/j.enbuild.2020.109755>.
- [18] A. Saeed, A. Al-Alili, A review on desiccant coated heat exchangers, *Sci. Technol. Built Environ.* 23 (2017) 136–150. <https://doi.org/10.1080/23744731.2016.1226076>.
- [19] C.C. Chang, C.H. Lai, C.M. Yang, Y.C. Chiang, S.L. Chen, Thermal performance enhancement of a periodic total heat exchanger using energy-storage material, *Energy Build.* 67 (2013) 579–586. <https://doi.org/10.1016/j.enbuild.2013.08.061>.
- [20] H. Ramin, E.N. Krishnan, W. Alabi, C.J. Simonson, Temperature Measurement Correction for the Determination of the Effectiveness of Fixed-Bed Regenerators (FBRs) for HVAC Applications, in: 2020 ASHRAE Annu. Summer Conf., ASHRAE, Austin, 2020.
- [21] H. Ramin, E.N. Krishnan, C.J. Simonson, Fixed bed regenerators for HVAC applications, 27th Can. Congr. Appl. Mech. (2019) 1–6. <https://doi.org/10.3390/proceedings2019023004>.
- [22] H. Ramin, E.N. Krishnan, A. Gurubalan, W.O. Alabi, J. Carey, A Transient Numerical Model for Sensible Fixed-Bed Regenerator in HVAC Applications, *Int. J.*

Heat Mass Transf. (n.d.).

- [23] E.N. Krishnan, H. Ramin, M. Shakouri, L.D. Wilson, C.J. Simonson, Development of a small-scale test facility for effectiveness evaluation of fixed-bed regenerators, *Appl. Therm. Eng.* 174 (2020) 115263.
<https://doi.org/10.1016/j.applthermaleng.2020.115263>.
- [24] H. Ramin, E.N. Krishnan, G. Annadurai, C.J. Simonson, Transient performance of fixed-bed regenerators for energy recovery in building applications, in: *Proc. ASME 2020 Heat Transf. Summer Conf. HT2020*, ASME, Orlando, Florida, 2020.
- [25] CSA Group, *CSA C439 Laboratory methods of test for rating the performance of heat / energy-recovery*, CSA Group, 2018.
- [26] ASHRAE, *BSR/ASHRAE Standard 84-2013R, Method of Testing Air-to-Air Heat/Energy Exchangers (First Public Review Draft)*, Atlanta, 2019.
- [27] H. Hashemian, *Measurement of Dynamic Temperatures and Pressures in Nuclear Power Plants*, Western University, 2011. <http://ir.lib.uwo.ca/etd/189/>.
- [28] S. Wang, J. Tang, F. Younce, Temperature Measurement, in: *Encycl. Agric. Food, Biol. Eng.*, Marcel Dekker, Inc, 2003: pp. 987–993. <https://doi.org/10.1081/E-EAFE>.
- [29] O.O. Abe, R.W. Besant, C.J. Simonson, W. Shang, Relationship between energy wheel speed and effectiveness and its transient response, part I: Mathematical development of the characteristic time constants and their relationship with effectiveness, in: *ASHRAE Trans.*, 2006: pp. 103–115.
- [30] Heat Recovery System | Heat Recovery Ventilator | ERV | Energy Recovery, (n.d.).
<https://www.tempeffnorthamerica.com/> (accessed July 12, 2019).
- [31] R.K. Shah, D.P. Sekulic, *Fundamentals of Heat Exchanger Design*, John Wiley &

- Sons, Inc., Hoboken, NJ, USA, 2003. <https://doi.org/10.1002/9780470172605>.
- [32] O. Buyukalaca, T. Yilmaz, Influence of rotational speed on effectiveness of rotary-type heat exchanger, *Heat Mass Transf.* 38 (2002) 441–447. <https://doi.org/DOI.10.1007/s002310100277>.
- [33] J. Seo, D. Lee, D. Kim, *International Journal of Heat and Mass Transfer* A simple effectiveness model for heat wheels, *Int. J. Heat Mass Transf.* 120 (2018) 1358–1364. <https://doi.org/10.1016/j.ijheatmasstransfer.2017.12.102>.
- [34] H. Versteeg, W. Malalasekera, *An Introduction to Computational Fluid Dynamics, The Finite Volume Method*, Pearson Education Limited, 2007. <https://doi.org/10.2514/1.22547>.
- [35] R.K. Shah, D.P. Sekulic, *Fundamentals of heat exchanger design*, New Jersey, 2004. <https://doi.org/10.1007/bf00740254>.
- [36] T.L. Bergman, A.S. Lavine, F.P. Incropera, D.P. Dewitt, *Fundamentals of heat and mass transfer, Seventh e*, John Wiley & Sons, INC., 2011.
- [37] E. Krishnan, H. Ramin, C.J. Simonson, Performance testing of fixed-bed regenerators for HVAC applications, in the *Second Pacific Rim Therm. Eng. Conf.*, Hawaii, 2019: pp. 1–5.
- [38] R.S. Figliola, D.E. Beasley, *Theory and Design for Mechanical Measurements*, 5th ed., John Wiley & Sons Inc, Hoboken, New Jersey, 2010. <https://doi.org/10.1017/CBO9781107415324.004>.
- [39] G.D. Bahnke, C.P. Howard, The effect of longitudinal heat conduction on periodic-flow heat exchanger performance, *J. Eng. Gas Turbines Power.* 86 (1964) 105–117. <https://doi.org/10.1115/1.3677551>.

**Appendix A: Effectiveness error from the transient response of sensors at
different operating conditions**

The following tables represent the error in effectiveness for different τ_s^* and λ values over the practical ranges of NTU_o and Cr^* .

Table A.1: Effectiveness error $\Delta\varepsilon$ (%) for $\lambda=0.0$.

		$\Delta\varepsilon$ (%) @ $\lambda=0.0$						
NTU_o	Cr^*	$\tau_s^*=0.01$	$\tau_s^*=0.02$	$\tau_s^*=0.05$	$\tau_s^*=0.1$	$\tau_s^*=0.2$	$\tau_s^*=0.3$	$\tau_s^*=0.5$
1.0	1.0	0.7	1.4	3.5	6.9	13.1	17.8	23.1
1.0	2.0	0.6	1.2	3.1	6.0	11.6	15.9	21.1
1.0	3.0	0.6	1.2	2.9	5.7	11.1	15.3	20.4
1.0	5.0	0.6	1.1	2.7	5.5	10.7	14.9	20.0
1.0	10.0	0.5	1.1	2.6	5.3	10.4	14.6	19.7
2.0	1.0	0.7	1.3	3.3	6.3	11.6	15.2	19.0
2.0	2.0	0.5	1.0	2.5	4.8	9.1	12.1	15.6
2.0	3.0	0.5	0.9	2.2	4.3	8.2	11.2	14.6
2.0	5.0	0.4	0.8	2.0	4.0	7.6	10.5	13.8
2.0	10.1	0.4	0.7	1.9	3.7	7.2	10.0	13.4
5.0	1.0	0.6	1.3	3.1	5.8	9.9	12.4	14.6
5.0	2.0	0.4	0.8	1.9	3.5	6.2	8.0	9.7
5.0	3.0	0.3	0.6	1.5	2.9	5.2	6.8	8.5
5.0	5.0	0.3	0.5	1.3	2.4	4.5	6.0	7.7
5.0	10.0	0.2	0.4	1.1	2.1	3.9	5.4	7.1
7.0	1.0	0.6	1.3	3.0	5.6	9.3	11.5	13.2
7.0	2.0	0.3	0.7	1.7	3.1	5.4	6.8	8.1
7.0	3.0	0.3	0.5	1.3	2.5	4.4	5.7	7.0
7.0	5.0	0.2	0.4	1.1	2.0	3.7	4.9	6.2
7.0	10.0	0.2	0.3	0.9	1.7	3.2	4.3	5.6
10.0	1.0	0.6	1.2	2.9	5.3	8.7	10.4	11.8
10.0	2.0	0.3	0.6	1.4	2.7	4.5	5.6	6.6
10.0	3.0	0.2	0.5	1.1	2.1	3.6	4.6	5.5
10.0	5.0	0.2	0.4	0.9	1.7	3.0	3.9	4.8
10.0	10.0	0.1	0.3	0.7	1.3	2.5	3.3	4.2

Table A.2: Effectiveness error $\Delta\varepsilon$ (%) for $\lambda=0.02$.

$\Delta\varepsilon$ (%) @ $\lambda=0.02$								
NTU _o	Cr*	$\tau_s^*=0.01$	$\tau_s^*=0.02$	$\tau_s^*=0.05$	$\tau_s^*=0.1$	$\tau_s^*=0.2$	$\tau_s^*=0.3$	$\tau_s^*=0.5$
1.0	1.0	0.7	1.4	3.5	6.9	13.1	17.8	23.1
1.0	2.0	0.6	1.2	3.1	6.0	11.6	16.0	21.2
1.0	3.0	0.6	1.2	2.9	5.7	11.1	15.4	20.5
1.0	5.0	0.6	1.1	2.8	5.5	10.7	14.9	20.1
1.0	10.0	0.5	1.1	2.7	5.3	10.5	14.6	19.8
2.0	1.0	0.7	1.4	3.3	6.4	11.7	15.4	19.2
2.0	2.0	0.5	1.0	2.5	4.9	9.2	12.3	15.8
2.0	3.0	0.5	0.9	2.3	4.4	8.4	11.4	14.8
2.0	5.0	0.4	0.8	2.0	4.0	7.8	10.7	14.1
2.0	10.1	0.4	0.8	1.9	3.7	7.3	10.2	13.6
5.0	1.0	0.7	1.3	3.1	5.8	10.1	12.7	15.1
5.0	2.0	0.4	0.8	1.9	3.6	6.5	8.3	10.2
5.0	3.0	0.3	0.6	1.6	3.0	5.5	7.2	9.0
5.0	5.0	0.3	0.5	1.3	2.5	4.8	6.4	8.2
5.0	10.0	0.2	0.5	1.1	2.2	4.2	5.7	7.6
7.0	1.0	0.6	1.3	3.1	5.7	9.6	11.9	13.8
7.0	2.0	0.4	0.7	1.7	3.2	5.7	7.2	8.7
7.0	3.0	0.3	0.6	1.4	2.6	4.7	6.1	7.5
7.0	5.0	0.2	0.5	1.1	2.2	4.0	5.3	6.7
7.0	10.0	0.2	0.4	0.9	1.8	3.4	4.7	6.1
10.0	1.0	0.6	1.3	3.0	5.5	9.1	11.1	12.6
10.0	2.0	0.3	0.6	1.5	2.9	4.9	6.2	7.3
10.0	3.0	0.3	0.5	1.2	2.3	4.0	5.1	6.2
10.0	5.0	0.2	0.4	1.0	1.8	3.3	4.4	5.4
10.0	10.0	0.2	0.3	0.8	1.5	2.8	3.8	4.8

Table A.3: Effectiveness error $\Delta\varepsilon$ (%) for $\lambda=0.04$.

		$\Delta\varepsilon$ (%) @ $\lambda=0.04$						
NTU _o	Cr*	$\tau_S^*=0.01$	$\tau_S^*=0.02$	$\tau_S^*=0.05$	$\tau_S^*=0.1$	$\tau_S^*=0.2$	$\tau_S^*=0.3$	$\tau_S^*=0.5$
1.0	1.0	0.7	1.4	3.6	6.9	13.2	17.9	23.2
1.0	2.0	0.6	1.2	3.1	6.1	11.7	16.0	21.2
1.0	3.0	0.6	1.2	2.9	5.7	11.2	15.4	20.6
1.0	5.0	0.6	1.1	2.8	5.5	10.8	15.0	20.2
1.0	10.0	0.5	1.1	2.7	5.3	10.5	14.7	19.9
2.0	1.0	0.7	1.4	3.3	6.4	11.8	15.5	19.4
2.0	2.0	0.5	1.0	2.5	4.9	9.3	12.4	16.0
2.0	3.0	0.5	0.9	2.3	4.5	8.5	11.5	15.0
2.0	5.0	0.4	0.8	2.1	4.1	7.9	10.8	14.3
2.0	10.1	0.4	0.8	1.9	3.8	7.4	10.3	13.7
5.0	1.0	0.7	1.3	3.2	5.9	10.3	13.0	15.4
5.0	2.0	0.4	0.8	2.0	3.7	6.7	8.6	10.6
5.0	3.0	0.3	0.7	1.6	3.1	5.7	7.5	9.4
5.0	5.0	0.3	0.6	1.4	2.6	5.0	6.7	8.6
5.0	10.0	0.2	0.5	1.2	2.3	4.4	6.0	8.0
7.0	1.0	0.7	1.3	3.1	5.8	9.9	12.2	14.3
7.0	2.0	0.4	0.7	1.8	3.4	5.9	7.6	9.2
7.0	3.0	0.3	0.6	1.4	2.8	5.0	6.5	8.0
7.0	5.0	0.2	0.5	1.2	2.3	4.2	5.6	7.2
7.0	10.0	0.2	0.4	1.0	1.9	3.7	5.0	6.6
10.0	1.0	0.7	1.3	3.1	5.6	9.4	11.5	13.1
10.0	2.0	0.3	0.7	1.6	3.0	5.2	6.7	7.9
10.0	3.0	0.3	0.5	1.3	2.4	4.3	5.5	6.7
10.0	5.0	0.2	0.4	1.0	2.0	3.6	4.7	5.9
10.0	10.0	0.2	0.3	0.8	1.6	3.1	4.1	5.3

Table A.4: Effectiveness error $\Delta\varepsilon$ (%) for $\lambda=0.06$.

		$\Delta\varepsilon$ (%) @ $\lambda=0.06$						
NTU _o	Cr*	$\tau_s^*=0.01$	$\tau_s^*=0.02$	$\tau_s^*=0.05$	$\tau_s^*=0.1$	$\tau_s^*=0.2$	$\tau_s^*=0.3$	$\tau_s^*=0.5$
1.0	1.0	0.7	1.4	3.6	7.0	13.2	17.9	23.3
1.0	2.0	0.6	1.2	3.1	6.1	11.7	16.1	21.3
1.0	3.0	0.6	1.2	2.9	5.8	11.2	15.5	20.7
1.0	5.0	0.6	1.1	2.8	5.5	10.8	15.1	20.3
1.0	10.0	0.5	1.1	2.7	5.4	10.6	14.8	20.0
2.0	1.0	0.7	1.4	3.3	6.5	11.9	15.6	19.6
2.0	2.0	0.5	1.0	2.6	5.0	9.4	12.6	16.2
2.0	3.0	0.5	0.9	2.3	4.5	8.6	11.7	15.3
2.0	5.0	0.4	0.8	2.1	4.1	8.0	11.0	14.6
2.0	10.1	0.4	0.8	1.9	3.9	7.6	10.5	14.1
5.0	1.0	0.7	1.3	3.2	6.0	10.5	13.2	15.8
5.0	2.0	0.4	0.8	2.0	3.8	6.9	8.0	10.3
5.0	3.0	0.3	0.7	1.7	3.2	5.9	7.8	9.8
5.0	5.0	0.3	0.6	1.4	2.8	5.2	6.9	9.0
5.0	10.0	0.2	0.5	1.2	2.4	4.6	6.3	8.4
7.0	1.0	0.7	1.3	3.1	5.9	10.1	12.5	14.7
7.0	2.0	0.4	0.8	1.9	3.5	6.2	7.9	9.7
7.0	3.0	0.3	0.6	1.5	2.9	5.2	6.8	8.5
7.0	5.0	0.3	0.5	1.3	2.4	4.5	6.0	7.6
7.0	10.0	0.2	0.4	1.1	2.1	3.9	5.4	7.0
10.0	1.0	0.7	1.3	3.1	5.7	9.7	11.9	13.7
10.0	2.0	0.4	0.7	1.7	3.2	5.5	7.0	8.4
10.0	3.0	0.3	0.6	1.4	2.6	4.6	6.0	7.3
10.0	5.0	0.2	0.5	1.1	2.1	3.9	5.1	6.5
10.0	10.0	0.2	0.4	0.9	1.8	3.4	4.5	5.9

Table A.5: Effectiveness error $\Delta\varepsilon$ (%) for $\lambda=0.08$.

$\Delta\varepsilon$ (%) @ $\lambda=0.08$								
NTU _o	Cr*	$\tau_s^*=0.01$	$\tau_s^*=0.02$	$\tau_s^*=0.05$	$\tau_s^*=0.1$	$\tau_s^*=0.2$	$\tau_s^*=0.3$	$\tau_s^*=0.5$
1.0	1.0	0.7	1.4	3.6	7.0	13.3	18.0	23.4
1.0	2.0	0.6	1.2	3.1	6.1	11.8	16.2	21.4
1.0	3.0	0.6	1.2	2.9	5.8	11.3	15.6	20.8
1.0	5.0	0.6	1.1	2.8	5.6	10.9	15.1	20.4
1.0	10.0	0.5	1.1	2.7	5.4	10.6	14.8	20.1
2.0	1.0	0.7	1.4	3.4	6.5	11.9	15.7	19.7
2.0	2.0	0.5	1.1	2.6	5.0	9.5	12.7	16.4
2.0	3.0	0.5	0.9	2.3	4.6	8.7	11.8	15.5
2.0	5.0	0.4	0.9	2.1	4.2	8.1	11.1	14.8
2.0	10.1	0.4	0.8	2.0	3.9	7.7	10.6	14.3
5.0	1.0	0.7	1.3	3.2	6.0	10.6	13.5	16.1
5.0	2.0	0.4	0.8	2.1	3.9	7.1	9.2	11.4
5.0	3.0	0.4	0.7	1.7	3.3	6.1	8.1	10.2
5.0	5.0	0.3	0.6	1.5	2.9	5.4	7.2	9.4
5.0	10.0	0.3	0.5	1.3	2.5	4.8	6.6	8.8
7.0	1.0	0.7	1.3	3.2	5.9	10.2	12.8	15.1
7.0	2.0	0.4	0.8	1.9	3.6	6.4	8.3	10.1
7.0	3.0	0.3	0.6	1.6	3.0	5.4	7.1	8.9
7.0	5.0	0.3	0.5	1.3	2.5	4.7	6.3	8.1
7.0	10.0	0.2	0.4	1.1	2.2	4.2	5.7	7.4
10.0	1.0	0.7	1.3	3.1	5.8	9.9	12.2	14.2
10.0	2.0	0.4	0.7	1.8	3.3	5.8	7.4	9.0
10.0	3.0	0.3	0.6	1.4	2.7	4.9	6.3	7.8
10.0	5.0	0.2	0.5	1.2	2.3	4.2	5.5	7.0
10.0	10.0	0.2	0.4	1.0	1.9	3.6	4.9	6.4

Table A.6: Effectiveness error $\Delta\varepsilon$ (%) for $\lambda=0.12$.

$\Delta\varepsilon$ (%) @ $\lambda=0.12$								
NTU _o	Cr*	$\tau_s^*=0.01$	$\tau_s^*=0.02$	$\tau_s^*=0.05$	$\tau_s^*=0.1$	$\tau_s^*=0.2$	$\tau_s^*=0.3$	$\tau_s^*=0.5$
1.0	1.0	0.7	1.4	3.6	7.0	13.3	18.1	23.5
1.0	2.0	0.6	1.3	3.1	6.1	11.8	16.3	21.6
1.0	3.0	0.6	1.2	2.9	5.8	11.3	15.7	21.0
1.0	5.0	0.6	1.1	2.8	5.6	11.0	15.3	20.5
1.0	10.0	0.5	1.1	2.7	5.4	10.7	15.0	20.2
2.0	1.0	0.7	1.4	3.4	6.5	12.0	15.9	20.0
2.0	2.0	0.5	1.1	2.6	5.1	9.6	13.0	16.8
2.0	3.0	0.5	1.0	2.4	4.6	8.9	12.1	15.8
2.0	5.0	0.4	0.9	2.2	4.3	8.3	11.4	15.1
2.0	10.1	0.4	0.8	2.0	4.0	7.8	10.9	14.7
5.0	1.0	0.7	1.3	3.2	6.1	10.9	13.8	16.6
5.0	2.0	0.4	0.9	2.1	4.1	7.4	9.7	12.0
5.0	3.0	0.4	0.7	1.8	3.5	6.4	8.5	10.9
5.0	5.0	0.3	0.6	1.6	3.0	5.7	7.7	10.0
5.0	10.0	0.3	0.6	1.4	2.7	5.2	7.1	9.4
7.0	1.0	0.7	1.3	3.2	6.0	10.5	13.3	15.8
7.0	2.0	0.4	0.8	2.0	3.8	6.8	8.8	10.9
7.0	3.0	0.3	0.7	1.7	3.2	5.8	7.7	9.7
7.0	5.0	0.3	0.6	1.4	2.7	5.1	6.9	8.8
7.0	10.0	0.2	0.5	1.2	2.4	4.6	6.2	8.2
10.0	1.0	0.7	1.3	3.2	5.9	10.2	12.8	15.0
10.0	2.0	0.4	0.8	1.9	3.5	6.3	8.1	9.8
10.0	3.0	0.3	0.6	1.5	2.9	5.3	7.0	8.7
10.0	5.0	0.3	0.5	1.3	2.5	4.6	6.1	7.8
10.0	10.0	0.2	0.4	1.1	2.1	4.1	5.5	7.2

Table A.7: Effectiveness error $\Delta\varepsilon$ (%) for $\lambda=0.16$.

		$\Delta\varepsilon$ (%) @ $\lambda=0.16$						
NTU _o	Cr*	$\tau_S^*=0.01$	$\tau_S^*=0.02$	$\tau_S^*=0.05$	$\tau_S^*=0.1$	$\tau_S^*=0.2$	$\tau_S^*=0.3$	$\tau_S^*=0.5$
1.0	1.0	0.7	1.5	3.6	7.0	13.4	18.1	23.6
1.0	2.0	0.6	1.3	3.1	6.2	11.9	16.3	21.7
1.0	3.0	0.6	1.2	3.0	5.9	11.4	15.8	21.1
1.0	5.0	0.6	1.1	2.8	5.6	11.0	15.4	20.7
1.0	10.0	0.5	1.1	2.7	5.5	10.8	15.1	20.4
2.0	1.0	0.7	1.4	3.4	6.6	12.1	16.1	20.2
2.0	2.0	0.5	1.1	2.7	5.2	9.8	13.2	17.0
2.0	3.0	0.5	1.0	2.4	4.7	9.0	12.3	16.1
2.0	5.0	0.4	0.9	2.2	4.4	8.4	11.6	15.5
2.0	10.0	0.4	0.8	2.1	4.1	8.0	11.1	15.0
5.0	1.0	0.7	1.3	3.3	6.2	11.1	14.2	17.1
5.0	2.0	0.5	0.9	2.2	4.2	7.7	10.1	12.6
5.0	3.0	0.4	0.8	1.9	3.6	6.7	9.0	11.4
5.0	5.0	0.3	0.7	1.6	3.2	6.0	8.2	10.6
5.0	10.0	0.3	0.6	1.4	2.8	5.5	7.5	10.0
7.0	1.0	0.7	1.3	3.2	6.1	10.8	13.7	16.3
7.0	2.0	0.4	0.9	2.1	4.0	7.1	9.3	11.5
7.0	3.0	0.4	0.7	1.7	3.4	6.2	8.2	10.4
7.0	5.0	0.3	0.6	1.5	2.9	5.5	7.4	9.5
7.0	10.0	0.3	0.5	1.3	2.6	4.9	6.7	8.9
10.0	1.0	0.7	1.3	3.2	6.1	10.5	13.2	15.6
10.0	2.0	0.4	0.8	2.0	3.7	6.7	8.6	10.6
10.0	3.0	0.3	0.7	1.6	3.1	5.7	7.5	9.4
10.0	5.0	0.3	0.6	1.4	2.7	5.0	6.7	8.6

Table A.8: Effectiveness error $\Delta\varepsilon$ (%) for $\lambda=0.20$.

		$\Delta\varepsilon$ (%) @ $\lambda=0.20$						
NTU _o	Cr*	$\tau_s^*=0.01$	$\tau_s^*=0.02$	$\tau_s^*=0.05$	$\tau_s^*=0.1$	$\tau_s^*=0.2$	$\tau_s^*=0.3$	$\tau_s^*=0.5$
1.0	1.0	0.7	1.5	3.6	7.0	13.4	18.2	23.7
1.0	2.0	0.6	1.3	3.1	6.2	11.9	16.4	21.8
1.0	3.0	0.6	1.2	3.0	5.9	11.5	15.9	21.2
1.0	5.0	0.6	1.1	2.8	5.7	11.1	15.4	20.8
1.0	10.0	0.6	1.1	2.8	5.5	10.8	15.1	20.5
2.0	1.0	0.7	1.4	3.4	6.6	12.2	16.2	20.4
2.0	2.0	0.5	1.1	2.7	5.2	9.9	13.3	17.3
2.0	3.0	0.5	1.0	2.4	4.8	9.1	12.5	16.4
2.0	5.0	0.5	0.9	2.2	4.4	8.6	11.8	15.7
2.0	10.1	0.4	0.8	2.1	4.2	8.2	11.4	15.3
5.0	1.0	0.7	1.4	3.3	6.3	11.2	14.4	17.5
5.0	2.0	0.5	0.9	2.3	4.3	7.9	10.4	13.1
5.0	3.0	0.4	0.8	1.9	3.8	7.0	9.3	12.0
5.0	5.0	0.3	0.7	1.7	3.3	6.3	8.5	11.1
5.0	10.0	0.3	0.6	1.5	3.0	5.8	7.9	10.5
7.0	1.0	0.7	1.3	3.3	6.2	11.0	14.0	16.8
7.0	2.0	0.4	0.9	2.1	4.1	7.4	9.7	12.1
7.0	3.0	0.4	0.7	1.8	3.5	6.5	8.6	11.0
7.0	5.0	0.3	0.6	1.6	3.1	5.8	7.8	10.1
7.0	10.0	0.3	0.6	1.4	2.7	5.2	7.2	9.5
10.0	1.0	0.7	1.3	3.3	6.1	10.7	13.6	16.2
10.0	2.0	0.4	0.8	2.1	3.9	7.0	9.1	11.3
10.0	3.0	0.4	0.7	1.7	3.3	6.1	8.0	10.1
10.0	5.0	0.3	0.6	1.5	2.9	5.4	7.2	9.3

Table A.9: Effectiveness error $\Delta\varepsilon$ (%) for $\lambda=0.24$.

		$\Delta\varepsilon$ (%) @ $\lambda=0.24$						
NTU _o	Cr*	$\tau_s^*=0.01$	$\tau_s^*=0.02$	$\tau_s^*=0.05$	$\tau_s^*=0.1$	$\tau_s^*=0.2$	$\tau_s^*=0.3$	$\tau_s^*=0.5$
1.0	1.0	0.7	1.5	3.6	7.1	13.4	18.2	23.7
1.0	2.0	0.6	1.3	3.1	6.2	12.0	16.5	21.9
1.0	3.0	0.6	1.2	3.0	5.9	11.5	15.9	21.3
1.0	5.0	0.6	1.1	2.9	5.7	11.1	15.5	20.9
1.0	10.0	0.6	1.1	2.8	5.5	10.9	15.2	20.6
2.0	1.0	0.7	1.4	3.4	6.6	12.3	16.3	20.6
2.0	2.0	0.6	1.1	2.7	5.3	10.0	13.5	17.5
2.0	3.0	0.5	1.0	2.5	4.8	9.3	12.6	16.6
2.0	5.0	0.5	0.9	2.3	4.5	8.7	12.0	16.0
2.0	10.1	0.4	0.9	2.1	4.2	8.3	11.5	15.5
5.0	1.0	0.7	1.4	3.3	6.3	11.4	14.7	17.9
5.0	2.0	0.5	0.9	2.3	4.4	8.1	10.7	13.5
5.0	3.0	0.4	0.8	2.0	3.9	7.2	9.7	12.4
5.0	5.0	0.4	0.7	1.8	3.4	6.5	8.7	11.6
5.0	10.0	0.3	0.6	1.6	3.1	6.0	8.3	11.0
7.0	1.0	0.7	1.4	3.3	6.3	11.1	14.3	17.2
7.0	2.0	0.5	0.9	2.2	4.2	7.7	10.1	12.6
7.0	3.0	0.4	0.8	1.9	3.6	6.8	9.0	11.5
7.0	5.0	0.3	0.7	1.6	3.2	6.1	8.2	10.7
7.0	10.0	0.3	0.6	1.5	2.9	5.5	7.6	10.0
10.0	1.0	0.7	1.4	3.3	6.2	10.9	13.9	16.6
10.0	2.0	0.4	0.9	2.1	4.0	7.3	9.5	11.9
10.0	3.0	0.4	0.7	1.8	3.4	6.4	8.4	10.7
10.0	5.0	0.3	0.6	1.5	3.0	5.7	7.6	9.9

Example A.1:

This example demonstrates the impact of temperature sensor on the system performance. Consider a space that requires 10,000 CFM of ventilation air to meet the outdoor air requirements. Heat exchanger design parameters and operation conditions, as well as the sensor time constant, are presented in Table A.1.

Table A.1: design and operating conditions

NTU	Cr*	λ	Indoor design temperature (°C)	Outdoor design temperature (°C)	Recovery period (s)	Sensor time constant
5	3	0.04	24	-5	30	6

For this condition, the actual effectiveness of the heat exchanger is 80.2%, and the recovered heat would be 13.5kW. With temperature sensors with a time constant of 6 seconds, the measured effectiveness is 85.9% (from Table A.3), and hence the predicted recovered heat would be 14.5kW. Therefore the measured values overpredict the recovered heat by 1kW at the mentioned conditions. If this sensor is located in the buildings, the inaccurate measurements caused the systems to add less heat to the supply air and could deteriorate the thermal comfort within the building.

It should be noted that in an actual building, there are other thermal masses in the system that might affect the temperature profile that occupant experiences. This model, however, considers the sensor time constant and its effect on the measured temperature and effectiveness at the outlet of the exchanger only.